Resilient CD8$^+$ T cells maintain a high cytotoxic capacity by balancing ROS via ME1 upregulation

Joanina K. Gicobi[1], Zhiming Mao[1], Grace DeFranco[1], Ying Li[3], Xin Liu[2], Jacob B. Hirdler[2], Vianca V. Vianzon[1], Emilia R. Dellacecca[1], Michelle A. Hsu[1], Whitney Barham[1], Yohan Kim[2], Feven Abraha[4], William S. Harmsen[4], Yiyi Yan[5], Roxana S. Dronca[5], Mojun Zhu[6], Svetomir N. Markovic[6], Aaron S. Mansfield[6], Yi Lin[6], Xiaosheng Wu[6], Dawn Owen[7], Michael P. Grams[7], Jacob J. Orme[6], Fabrice Lucien[2], Hu Zeng[1, 8], Sean S. Park[7], Haidong Dong[1, 2, *]

[1] Department of Immunology, Mayo Clinic College of Medicine and Science, Rochester, MN
[2] Department of Urology, Mayo Clinic, Rochester, MN
[3] Department of Biomedical Statistics and Informatics, Mayo Clinic, Rochester, MN
[4] Department of Quantitative Health Sciences, Mayo Clinic, Rochester, MN
[5] Division of Medical Oncology, Mayo Clinic, Jacksonville, FL
[6] Division of Medical Oncology, Mayo Clinic, Rochester, MN
[7] Department of Radiation Oncology, Mayo Clinic, Rochester, MN
[8] Department of Rheumatology, Mayo Clinic, Rochester, MN

[*]Corresponding Author: dong.haidong@mayo.edu

Graphical abstract

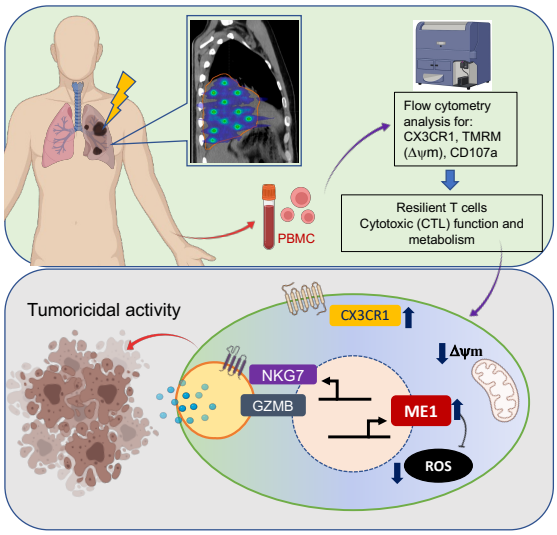

Highlights

- CX3CR1$^+$ and low Δψm identify functional resilient CD8$^+$ T cells.
- Resilient CD8$^+$ T cells are highly cytotoxic and have less ROS.
- Resilient CD8$^+$ T cells express more ME1 that can balance extra ROS.
- ME1 overexpression can promote CTL function of CD8$^+$ T cells.

Abstract

Cytotoxic T lymphocytes (CTL) are indispensable in anti-tumor immunity. Although CTLs are prone to exhaustion in patients with advanced cancer, T cell resiliency explains the presence of tumor-reactive CTLs that are less exhausted, capable of cytolytic function, expansion, and rebound in response to immunotherapy to reject metastatic malignances. However, the features of resilient T cells have not been clearly defined. In this report, we demonstrate that peripheral CX3CR1$^+$ CD8$^+$ T cells with low mitochondrial membrane potential rebounded CTL function quickly after radiation therapy in patients with large tumor burden portraying their functional resiliency. Furthermore, CX3CR1$^+$ CD8$^+$ T cell with low, but not high, mitochondrial membrane potential are highly cytotoxic, accumulate less reactive oxygen species (ROS), and express more Malic enzyme 1 (ME1). ME1 overexpression increases ATP production in a glycolysis-independent manner while concurrently curtailing excessive ROS in activated CD8$^+$ T cells; and expands CX3CR1$^+$NKG7$^+$ effector CD8$^+$ T cells with enhanced cytotoxicity. Importantly, transfection of *ME1* mRNA promotes tumoricidal activity in CD8$^+$ T cells from patients with advanced cancers. Our study reveals a mechanism used by CTLs to balance excessive ROS via ME1 to maintain a metabolic and functional resiliency. Modification of ME1 expression in CTLs may be a novel method to improve the efficacy of cancer immunotherapy by preventing T cell exhaustion.

Introduction.

Immunotherapies (immune checkpoint inhibitors (ICI), vaccines, or T cell therapies) are dependent on the presence of endogenous cytotoxic T lymphocytes (CTLs) to respond to ICI or to provide a substrate for adoptive cell transfer therapy[1]. Moreover, radiation therapy has been used frequently to reduce the tumor burden and to create opportunity for immunotherapy synergy[2]. To that end, the functionality of endogenous tumor-reactive CTLs plays a key role in predicting clinical response to combined radiation and immunotherapy[3,4].

Recently, we have proposed the term "resilient T cells" (Trs) to describe a functional state of tumor-reactive cytotoxic T cells that are capable of responding to immunotherapy by withstanding tumor burden and enduring the harsh conditions of the tumor microenvironment [5,6]. From there, a computational model of T cell resilience in multiple tumor types has been established to predict whether a cancer immunotherapy will be effective in certain patients [7]. However, it is not clear whether Trs cells can be identified in the circulation of patients with large tumor burden (5-10 cm or more in diameter). Of note, the identification and characterization of circulating Trs cells in these patients is pivotal to clinical treatment plans because the presence of Trs cells is the foundation for the control of advanced cancer by combination immunotherapy.

It has been reported that successful ICI therapy expands tumor-reactive CD8$^+$ T cells with an effector phenotype in the peripheral blood, which have the potential to replace exhausted T cells inside tumor tissue [8-12]. To that end, we and others identified CX3CR1$^+$ CD8$^+$ T cells that are responsive to ICI therapy in both preclinical and clinical setting [11,13,14]. Because CX3CR1$^+$ CD8$^+$ T cells are highly cytotoxic, proliferative, and active in preclinical models and in the peripheral blood of patients who respond to ICI therapy [10,11,13], we hypothesize that CX3CR1$^+$

$CD8^+$ T cells are prototypes of Trs cells in the circulation of patients with advanced cancers. A further characterization of $CX3CR1^+$ $CD8^+$ T cells will provide insights into the biology of Trs cells in circulation.

In this report, we found that post-radiation therapy in patients with advanced cancer, $CX3CR1^+$ $CD8^+$ T cells with low mitochondrial membrane potential ($\Delta\Psi m$) undergo a rapid cytotoxic response. Upon further characterization of $CD8^+$ T cells with low $\Delta\Psi m$, we found that they are highly cytotoxic and accumulate less ROS (reactive oxygen species) but express more Malic enzyme 1 (ME1) compared to T cells with high $\Delta\Psi m$. From there, we found that ME1 acts as an anti-oxidant in $CD8^+$ T cells and expands $CX3CR1^+$ $NKG7^+$ effector $CD8^+$ T cells with enhanced cytotoxicity. Importantly, ME1 overexpression introduced by *ME1* mRNA also increases mitochondrial-linked ATP while curtailing excessive ROS, thus enhancing the tumoricidal activity in $CD8^+$ T cells from patients with advanced cancers. Our study suggests that resilient T cells balance excessive ROS upon antigen stimulation via upregulation of ME1 to maintain their metabolic fitness and retain a high cytotoxic capacity. Modification of ME1 expression in T cells may be a new method to avoid T cell exhaustion and improve the efficacy of cancer immunotherapy.

Results

CX3CR1 and low mitochondria membrane potential identify resilient $CD8^+$ T cells in patients with advanced cancers

To reduce the tumor burden in patients with very large (5-10 cm or larger in diameter) or therapy-resistant tumors, patients were treated with a unique form of radiation therapy, spatially fractionated radiotherapy (SFRT) (**Fig. 1a**). SFRT is unique in that it intentionally delivers a heterogeneous dose distribution providing alternating regions of very high and low doses throughout the tumor[15]. SFRT can produce dramatic relief of severe symptoms, cause significant tumor regression, and achieve above average local control rates [16]. The biologic mechanisms responsible for the effectiveness of SFRT are still unknown, but the heterogeneous dose distribution is hypothesized to be responsible for modifying tumor-reactive immune responses both locally and systemically.

We and others previously identified circulating $CX3CR1^+$ $CD8^+$ T cells that are less exhausted and demonstrate high cytotoxic capability in patients with advanced cancers such as melanoma and lung cancers [10,11,13]. We hypothesized that a change in the functional state of $CX3CR1^+$ $CD8^+$ T cells may reflect an optimal response to a successful SFRT. Given the presence of large tumor burden in these patients in which compromised mitochondrial function has been linked to T cell exhaustion [17-22], we measured the CTL function of $CX3CR1^+$ $CD8^+$ T cells along with their mitochondrial membrane potential ($\Delta\Psi m$) to determine their mitochondrial function. The CTL function of these T cells was measured by CD107a expression, which reflects degranulation and cytotoxicity. In lung cancer and sarcoma patients with large tumor burden, $CX3CR1^+$ $CD8^+$ T cells with low, but not high $\Delta\Psi m$ showed improved CTL function one day after SFRT (**Fig. 1a-c, Extended Data Fig. 1a**). Similarly, one week after SFRT we found $CD8^+$ T cells with low $\Delta\Psi m$ showed improved CTL function compared to cells with high $\Delta\Psi m$ (**Fig. 1d**). In another cohort of patients with advanced melanoma whom were resistant to ICI therapy, we found that

CX3CR1$^+$ CD8$^+$ T cells, but not CX3CR1$^-$ CD8$^+$ T cells, exhibit a low ΔΨm phenotype in the peripheral blood (**Fig. 1d**) prior to radiation therapy. We treated this cohort of patients with stereotactic body radiotherapy (SBRT) to reduce tumor burden. From there, we found patients with a higher frequency (>28%, cut-off line indicated in **Fig. 1e**) of CX3CR1$^+$ CD8$^+$ T cells with low ΔΨm at baseline demonstrated superior overall survival (OS) in response to SBRT (**Fig. 1f**). On the other hand, we found a gradually decreasing frequency of CX3CR1$^+$ CD8$^+$ T cells with low ΔΨm in responders to ICI therapy as the tumor burden reduced, but fluctuating frequency in non-responders and persistence of tumor burden (**Extended Data Fig. 1b-c**). Taken together our clinical observations suggest that CX3CR1$^+$ CD8$^+$ T cells with low ΔΨm are present in patients with large tumor burdens, and demonstrate a resiliency in their cytotoxic function after radiation therapy.

Resilient CD8$^+$ T cells are highly cytotoxic and less exhausted

Although murine CD8$^+$ T cells with low ΔΨm demonstrates a higher antitumor activity [23], the cytotoxic functionality of human CD8$^+$ T cells with low or high ΔΨm has not been clearly defined. To understand whether the low ΔΨm feature of CD8$^+$ T cells is associated with their functional state, we sorted CD8$^+$ T cells isolated from healthy donors into low or high ΔΨm using TMRM staining as reported [23] (**Fig. 2a; Extended Data Fig. 2a**). First, we performed bulk RNA-seq analysis to compare the transcriptional differences between CD8$^+$ T cells with low and high ΔΨm. We found CD8$^+$ T cells with low ΔΨm expressed more genes that code for cytotoxic effector molecules such as *GZMB, PRF1*, and *NKG7* than CD8$^+$ T cells with high ΔΨm (**Fig. 2b**). We then confirmed a higher expression of granzyme B in CD8$^+$ T cells with low ΔΨm compared to CD8$^+$ T cells with high ΔΨm using RT-PCR and flow cytometry (**Fig. 2c-d**). In a T cell-mediated tumor cytotoxicity assay following a brief T cell activation with anti-CD3/CD28, we found that CD8$^+$ T cells with low ΔΨm demonstrated 1.5-fold higher cytolytic activity compared to CD8$^+$ T cells with high ΔΨm in the killing of two tumor cell lines (breast cancer and prostate cancer) (**Fig. 2e**). Also, we observed significantly increased degranulation of CD8$^+$ T cells with low ΔΨm compared to CD8$^+$ T cells with high ΔΨm upon T cell activation (**Fig. 2f**). In addition, gene set enrichment analysis (GSEA) showed CD8$^+$ T cells with low ΔΨm are enriched for mediators of inflammatory responses including Interferon (IFN) and IL-2/STAT5 pathways (**Fig. 2g; Extended Data Fig. 2b**). We determined the phenotype of human CD8$^+$ T cells with low or high ΔΨm and found that CD8$^+$ T cells with low ΔΨm cells were enriched in both Temra-like (CCR7$^-$CD45RA$^+$) and Tnaive-like (CCR7$^+$CD45RA$^+$) subsets of CD8$^+$ T cells, indicating a limitation of using CCR7 and CD45RA to identify a functional state of resilient T cells (**Extended Data Fig. 2c**). Overall, our results suggest that human CD8$^+$ T cells with low ΔΨm are highly cytotoxic and more responsive to inflammatory signals.

Given the high cytotoxic capability of CD8$^+$ T cells with low ΔΨm, we investigated whether they are prone to exhaustion upon activation. Interestingly, CD8$^+$ T cells with low ΔΨm had lower expression of exhaustion markers such as TOX, a causative factor of T cell exhaustion[24] , and PD-1 (**Fig. 3a, b**) compared to cells with high ΔΨm. Interestingly, we found that CD8$^+$ T cells with low ΔΨm are enriched with a TCF-1$^+$PD-1$^+$ stem-like phenotype that has been reported to be responsive to immunotherapy (**Fig. 3c**) [23]. To confirm this possibility, we compared the cytotoxicity of CD8$^+$ T cells with low or high ΔΨm in a co-culture with anti-PD-1

or anti-PD-L1 antibody. We found the cytotoxicity of $CD8^+$ T cells with low ΔΨm increased in the presence of anti-PD-L1 or anti-PD-1 antibody compared to $CD8^+$ T cells with high ΔΨm, although only the anti-PD-L1 group reached a statistical significance (**Fig. 3d**). Additionally, a pathway analysis of our RNA-seq data revealed an enrichment for the anti-PD-1/L1 cancer immunotherapy pathway in $CD8^+$ T cells with low ΔΨm cells compared to high ΔΨm cells (**Extended Data Fig. 3a**). Since the transcription factors Eomesodermin (Eomes) and T-bet regulate the expression of effector genes in $CD8^+$ T cells [25-28] and the ratio of Eomes/T-bet may determine the state of T cell exhaustion and immune pathology [29,30], we measured and compared Eomes and T-bet expression between $CD8^+$ T cells with low or high ΔΨm. Although Eomes and T-bet expression at an mRNA level were significantly higher in $CD8^+$ T cells with low ΔΨm compared to high ΔΨm cells, the protein levels of Eomes and T-bet were comparable between $CD8^+$ T cells with low or high ΔΨm (**Fig. 3e-f**). These data suggest that although $CD8^+$ T cells with low ΔΨm seem to be programmed with a high capability of effector function that could lead to exhaustion (based on high Eomes transcription), their functional state may be regulated by alternative mechanisms preventing them from entering exhaustion.

Resilient $CD8^+$ T cells have lower glycolysis and less ROS

As the levels of ΔΨm of $CD8^+$ T cells reflect the metabolic state of T cells[23,31], we compared the usage of glycolysis, measured by extracellular acidification rates (ECAR), and mitochondrial respiration, measured by the oxygen consumption rates (OCR), between $CD8^+$ T cells with low ΔΨm or high ΔΨm. Effector $CD8^+$ T cells rapidly utilize glycolysis as a quick, but inefficient, means of ATP production to carry out their effector functions[32-34]. However, a recent report argues that activated human $CD8^+$ T cells increase their metabolic pathways in both glycolysis and oxidative phosphorylation [35]. We found $CD8^+$ T cells with low ΔΨm had lower glycolysis and glycolytic capacity than $CD8^+$ T cells with high ΔΨm (**Fig. 4a, b**), while their OCR was comparable between $CD8^+$ T cells with low ΔΨm or high ΔΨm (**Fig. 4c, d**). However, the OCR/ECAR ratio was higher in $CD8^+$ T cells with low ΔΨm compared to high ΔΨm cells (**Fig. 4f**), implying that the resilient $CD8^+$ T cells may utilize more mitochondrial respiration for energy needs instead of glycolysis. Accordingly, mitochondrial-linked ATP and spare respiratory capacity were comparable between $CD8^+$ T cells with low ΔΨm and high ΔΨm (**Fig. 4d, f).** Given the high cytotoxic capacity of $CD8^+$ T cells with low ΔΨm, it is unexpected that they would exhibit low glycolysis. Since GLUT1 levels were comparable between $CD8^+$ T cells with low ΔΨm and high ΔΨm (**Fig. 4g**), it is possible that the lower glycolysis of $CD8^+$ T cells with low ΔΨm is not due to a lower intake of glucose, but rather a preference for lower lactate production via glycolysis which could result in Warburg effects that limit their functionality[36]. Our data suggests that $CD8^+$ T cells with low ΔΨm do not have increased glycolysis, but rather meet their energy requirements via mitochondrial-linked respiration.

Consistent with our observations above, our GSEA analysis shows that the ROS pathway was enriched in $CD8^+$ T cells with high ΔΨm compared to those with low ΔΨm (**Fig. 5a**). To confirm this finding, we directly measured ROS levels in $CD8^+$ T cells with low ΔΨm or high ΔΨm. We found both cytosolic ROS and mitochondrial ROS to be lower in resting and activated $CD8^+$ T cells with low ΔΨm compared to $CD8^+$ T cells with high ΔΨm (**Fig. 5b-c**), and that these lower levels of ROS were maintained for up to 7 days during the *in vitro* culture (**Fig. 5c**).

To that end, we measured and compared the mass and numbers of mitochondria between $CD8^+$ T cells with low and high ΔΨm. Although there was a trend for decreased mitochondrial mass and numbers of mitochondria in $CD8^+$ T cells with low ΔΨm (**Fig. 5d-e**), this difference did not reach statistical significance, suggesting other mechanisms, beyond mitochondrial volume, may contribute to the lower levels of ROS.

Since excessive ROS signals result in DNA damage and functional exhaustion in T cells [22,37,38], the ability to maintain a lower ROS level, in the context of a higher OCR/ECAR ratio, could be a unique feature of resilient $CD8^+$ T cells with low ΔΨm. Harsh tumor microenvironments lead to increased ROS in T cells, but $CD8^+$ T cells with low ΔΨm may be enabled to tolerate these conditions. To test whether this feature is retained in T cells from patients with large tumor burdens, we measured and compared the levels of ROS in $CD8^+$ T cells with low or high ΔΨm isolated from patients with advanced lung cancers and sarcoma before and after SFRT. Interestingly, a lower level of ROS was consistently maintained in $CD8^+$ T cells with low ΔΨm compared to cells with high ΔΨm before and after SFRT (**Fig. 5f,** n=9). Similar findings were confirmed in another cohort of patients with advanced prostate cancer receiving SBRT (**Fig. 5f,** n=21). Taken together, our results suggest that $CD8^+$ T cells with low ΔΨm selectively use mitochondrial respiration to meet their energy needs but have a capability to balance ROS levels to avoid an excessive ROS accumulation.

ME1 is upregulated in Resilient $CD8^+$ T cells

To determine how $CD8^+$ T cells with low ΔΨm can maintain their ATP production via mitochondrial respiration, while also keeping a lower ROS level, we performed RNA-seq analysis and found ME1 to be among the most upregulated genes in the $CD8^+$ T cells with low ΔΨm cells in both resting and activated states compared to $CD8^+$ T cells with high ΔΨm (**Fig. 6a-b**). Since ME1 alone has the potential to regulate metabolism and ROS among these upregulated genes[39,40], we focused on ME1 and confirmed its higher expression in $CD8^+$ T cells with low ΔΨm cells compared to high ΔΨm cells via quantitative RT-PCR and Western blot in both resting and activated $CD8^+$ T cells (**Fig. 6c-d**).

To examine the consequence of ME1 expression in $CD8^+$ T cells with low or high ΔΨm, we sorted $CD8^+$ T cells with low or high ΔΨm from healthy donors followed with ME1 mRNA transfection and functional analysis (**Fig. 6e**). The overexpression of ME1 was confirmed by RT-PCR (**Fig. 6f**). Interestingly, we found that ME1 overexpression reduced ROS levels only in $CD8^+$ T cells with high ΔΨm, but not in $CD8^+$ T cells with low ΔΨm (**Fig. 6g**). Of note, although ME1 has the capability to reduce ROS levels in $CD8^+$ T cells, ME1 did not completely abolish ROS there, suggesting ME1 is a regulator of ROS rather than a scavenger of ROS in T cells. Since a basal level of ROS is also required for T cell activation[41], we determined whether ME1 overexpression would affect the functionality of $CD8^+$ T cells. To do so, we measured and compared the T cell-mediated cytotoxicity between $CD8^+$ T cells transfected with control or ME1 mRNA. The overexpression of ME1 in $CD8^+$ was confirmed via western blot (**Extended Data Fig. 4a-b**). Interestingly, we found that ME1 overexpression significantly increased the cytotoxicity of $CD8^+$ T cells against tumor cells *in vitro* (**Fig. 6h**). Accordingly, we found ME1 overexpression significantly increased the frequency of highly cytotoxic $CX3CR1^+$ $NKG7^+$ $CD8^+$ T cells [42] upon T cell activation (**Fig. 6i**). Our results suggest that ME1 may not only regulate the

level of ROS in $CD8^+$ T cells according to their mitochondrial potential, but also enhance CTL functionality.

ME1 increases metabolic output of $CD8^+$ T cells without increasing ROS

To understand how ME1 enhances CTL function of $CD8^+$ T cells, we examined whether ME1 regulates T cell metabolism upon activation, being that ME1 is a cytosolic enzyme that converts malate into pyruvate and produces NAPDH[39,40]. Interestingly, we found that $CD8^+$ T cells with ME1 overexpression had higher basal and maximal respiration, as well as a higher ATP-linked respiration, but their spare respiratory capacity did not increase significantly (**Fig. 7a; Extended Data Fig. 4c**). On the other hand, we found that ME1 overexpression did not affect the glycolysis and glycolytic capacity in $CD8^+$ T cells (**Fig. 7b**). Importantly, the increased mitochondrial respiration induced by ME1 overexpression did not result in an elevated level of cytosolic ROS among total $CD8^+$ T cells at either the activation or resting stage (**Fig. 7c; Extended Data Fig. 4d**).

To test whether ME1 may have a therapeutic potential in improving CTL function of PBMCs in patients with large tumor burdens, we introduced ME1 mRNA into PBMCs isolated from patients with advanced melanoma and prostate cancer. We found that ME1 overexpression increased the tumor killing ability of PBMCs in about 50% of patients with either cancer (**Fig. 7d**). From there, we found that ME1 overexpression reduced ROS only in $CD8^+$ T cells with low $\Delta\Psi m$ but not in high $\Delta\Psi m$ cells (**Fig. 7e**), suggesting $CD8^+$ T cells with low $\Delta\Psi m$ in patients with large tumor burdens could be more sensitive to regulation mediated by ME1 overexpression. Taken together, our results imply that ME1 can promote CTL function in activated CD8+ T cells via increased cellular ATP production and mitochondrial activity, allowing energy requirements to be met, while concurrently curtailing excessive ROS, thereby preventing exhaustion (**Fig. 7f**).

Discussion

In this study, we characterized the features of resilient T cells in patients with advanced malignancies. We found $CX3CR1^+$ $CD8^+$ T cells with low $\Delta\Psi m$ to be endowed with functional resiliency and metabolic fitness that allows them to withstand large tumor burden, retain cytotoxic functionality, and be responsive to radiation therapy or ICI treatment. One potential underlying mechanism of this resiliency is the upregulation of ME1 that not only balances excessive ROS in activated T cells, but also sufficiently enhances cytotoxic T cell responses. Thus, our study reveals a mechanism by which a highly cytotoxic function can be maintained in resilient T cells in patients with large tumor burdens and provides a method to improve the efficacy of cancer immunotherapy and radiation therapy for patients with advanced cancer.

Since PD-1 signals dynamically influence mitochondrial functions resulting in compromised function of effector T cells along with large tumor burdens[17-22], we measured the mitochondrial membrane potential ($\Delta\Psi m$) of $CX3CR1^+$ $CD8^+$ T cells to determine the functional state of their mitochondria, as a start to understanding T cell resilience. According to the level of $\Delta\Psi m$, we found $CX3CR1^+$ $CD8^+$ T cells with low $\Delta\Psi m$ to be more responsive to radiation therapy in

patients with large tumor burdens. From there, we further characterized $CD8^+$ T cells with low ΔΨm and found that they are highly cytotoxic and produce less ROS. We found that ME1 is upregulated in $CD8^+$ T cells with low ΔΨm and is responsible for balancing elevated levels of ROS in activated T cells and consequently promoting tumoricidal activity of $CD8^+$ T cells in both healthy donors and patients with advanced cancers. To our knowledge, the role of ME1 in T cell function has not been clearly defined, although ME1 has been identified as a key tumorigenic factor by promoting the survival of tumor cells in their microenvironment where high ROS is prevalent [39,43]. ME1 is an NADP+ dependent cytosolic enzyme that is required for catalytic activity of a reaction that converts malate into pyruvate with NAPDH as a by-product[39,40]. This means that the catalytic function of ME1 in $CD8^+$ T cells with low ΔΨm may serve to provide pyruvate, which feeds into either glycolytic or oxidative phosphorylation pathways for ATP production, and thus providing an optimal maintenance of metabolic fitness in T cells. Additionally, NADPH produced from the ME-1-mediated reaction can act as an anti-oxidant to prevent accumulation of excessive ROS, which may trigger T cell death [44] and T cell exhaustion [22,37,38]. Of note, although ME1 has the potential to reduce cytosolic ROS, probably through NADPH, our data suggest ME1 is not a scavenger of cytosolic or mitochondrial ROS in T cells that require a basal level of ROS for activation[41].

Large tumor burden has been significantly correlated with more T cells exhaustion and poorer response to ICI therapy [45,46]. However, the presence of resilient T cells that can recover their CTL function quickly after radiation therapy is an unexpected discovery in our study. Although the concept of resilient T cells in response to cancer immunotherapy has been conceived recently [5-7], no markers have been defined to identify them in patients with advanced diseases. To that end, our study suggest that $CX3CR1^+$ $CD8^+$ T cells with low ΔΨm could be a surrogate of resilient T cells, based on several features we identified in this report, such as (1) the quick recovery of their CTL function (degranulation/CD107a expression) after reduction of tumor burden by radiation therapy; (2) the maintenance of a low glycolytic profile, but production of optimal ATP levels; (3) the avoidance of exhaustion due to lower expression of PD-1 and TOX; (4) the shared feature of stem-like T cells ($TCF1^+PD\text{-}1^+$) which can be responsive to ICI therapy[47-52], which is consistent with murine $CD8^+$ T cells with low ΔΨm [23]; (5) the maintenance of a relatively lower ROS level, to avoid exhaustion while not compromising T cell activation[41]; (6) the upregulation of ME1 expression, effectively balancing excessive ROS and contributing to expansion of highly cytotoxic effector T cells. These unique features of resilient T cells can not only be used as a T cell biomarker to predict or monitor patient responses to cancer immunotherapy or combination therapy, but also can be used to convey a resilient functional state of T cells in patients who may be lacking enough resilient T cells required for immunotherapeutic response. To that end, our study suggests that introduction of ME1 mRNA into T cells could be used to improve the efficacy of cancer immunotherapy either in response to ICI therapy or in adoptive T cell therapy.

Several limitations in our studies should be addressed in future studies. Although our current studies are mainly focused on the circulating $CD8^+$ T cells in patients with advanced diseases, it is warranted to investigate whether tumoral $CD8^+$ T cells share the features of resilient T cells. On the other hand, since there are no animal models to address the T cell-specific role of ME1 in antitumor immunity, new animal models of ME1 are needed to test how a persistent or transient expression of ME1 in tumor-reactive T cells would contribute to either endogenous tumor

control or to response of ICI therapy. Also, the efficacy and safety of transferring ME1-modified T cells in treatment of established tumors would still need to be addressed by *in vivo* murine tumor experiments. Finally, one open question remains as to why some $CD8^+$ T cells are endowed with or maintain a low or high ΔΨm status. It is not clear to what degree the heterogeneity of ΔΨm within human circulating $CD8^+$ T cells would be related to systemic antitumor immunity, as resilient T cells need to maintain a depolarized low ΔΨm to avoid the consequences associated with high ΔΨm, such as increased ROS or exhaustion. By adapting to this unique feature, resilient T cells can protect the organism from metastatic cancer and chronic viral infections.

In summary, our study identified a mechanism by which resilient T cells can avoid exhaustion in patients with advanced cancers. Leveraging the knowledge of T cell resiliency may improve the efficacy of ICI, CAR-T cell, or TCR-T cell therapies to control metastatic malignancies that require robust systemic anti-tumor immunity for their control.

FIGURES

Fig. 1: CX3CR1 and low ΔΨm identifies resilient CD8 T cells in patients with advanced cancers upon radiation therapy. a, A diagram of spatially fractionated radiotherapy (SFRT) therapy and study design for **b-c**. **b,** Degranulation assay (measured by CD107a expression) of $CX3CR1^+$ $CD8^+$ T cells with low or high ΔΨm. **c-d**, Summaries of percentages of $CD107a^+$ cells among $CX3CR1^+CD8^+$ T cells with low or high ΔΨm from patients with advanced lung cancer and sarcoma (n=17) at baseline and 24 hours (hrs) post SFRT therapy (c), and one week (wk) post SFRT (d). Each line indicates one individual patient. **e,** Percentages of $CX3CR1^+$ (left) and $CX3CR1^-$ (right) $CD8^+$ T cells with low or high ΔΨm from patients with melanoma receiving SBRT at baseline. **f,** Survival probabilities at baseline prior to stereotactic body radiotherapy (SBRT) in patients (n=20) with advanced melanoma. Kaplan-Meier estimates were used to estimate survival curves and a univariate Cox model was used to determine the association of patients and disease variables with the risk of each outcome of interest. Statistical significance was determined by Student's Paired two-tailed t-test in **b-c**, and non-paired t-test in **d**, *P<0.05, **P<0.01, ****P<0.0001, ns: not significant.

Extended Data Fig. 1: Functionality and frequency of $CX3CR1^+$ $CD8^+$ T cells with low or high ΔΨm in response to radiation or ICI therapy. a, Degranulation analysis of $CX3CR1^+$ $CD8^+$ T cells with high ΔΨm from patients with advanced lung cancer and sarcoma (n=17) as measured by CD107a expression comparing baseline and 24 hours (hrs) post-spatially fractionated radiotherapy (SFRT) therapy. Frequency of $CX3CR1^+$ $CD8^+$ T cells with low ΔΨm was measured in the peripheral blood of patients with advanced melanoma at baseline (BL) and follow up time points (N=42) in responders (**b**) and non-responders (**c**) to Immune checkpoint inhibitors (ICI) therapy. Statistical significance was determined by Student's Paired two-tailed t-test in **a** *P<0.05, ns: not significant.

Fig. 2: Resilient CD8 T cells have high cytolytic capability. a, Experimental schematic. **b,** Heatmap of differentially expressed genes from bulk RNA-sequencing (RNA-seq) of anti-CD3/CD28 activated CD8+ T cells sorted according to low and high ΔΨm (N=3). Framed area

indicates genes that encode cytotoxic molecules**. c,** Relative GZMB mRNA expression in 5 donors. **d,** Expression of granzyme B protein in activated $CD8^+$ T cells with low or high ΔΨm as analyzed by flow cytometry for MFI (median fluorescent intensity) and percentage of positive cells. **e,** Cytotoxicity assay of $CD8^+$ T cells with low or high ΔΨm against tumor cells (MCF-7 breast and PC.3 prostate cancer) at a ratio of 1:20 (tumor:effector) in a 4-hour Calcein release assay (n=9-10). **f,** Degranulation assay of $CX3CR1^+$ $CD8^+$ T cells with low or high ΔΨm as measured by CD107a expression. **g,** Hallmark Gene Set Enrichment Analysis (GSEA) of RNA-seq data from three healthy donors using IPA analysis software. Statistical significance was determined by Student's paired (**f**) or non-paired (**c-e**) two-tailed t-test, *P<0.05, **P<0.01.

Extended Data Fig. 2: Sorting and phenotype analysis of $CD8^+$ T cells with low or high ΔΨm. a, Gating strategy that defines the low and high ΔΨm among $CD8^+$ T cells for sorting and analysis. **b,** Hallmark Gene Set Enrichment Analysis (GSEA) of RNA-sequencing data from three healthy donors using IPA analysis software. **c,** Phenotype of $CD8^+$ T cell subsets as defined by CCR7 and CD45RA expression among low or high ΔΨm cells. Statistical significance was determined by Student's Paired two-tailed t-test in **c,** **P<0.01, ***P<0.001, ****P<0.0001.

Fig. 3: Resilient CD8 T cells are not prone to be exhausted. a-b, TOX (a) and PD-1 (b) expression by activated $CD8^+$ T cells with low and high ΔΨm as analyzed by flow cytometry in median fluorescent intensity (MFI) and frequency (%). **c,** Frequency of TCF-1^+ PD-1^+ among $CD8^+$ T cells with low or high ΔΨm at activated state. **d,** $CD8^+$ T cells with low or high ΔΨm were activated with anti-CD3/CD28 beads in the presence of anti-PD-1 (Pembro) or anti-PD-L1 (Atezo) for 72 hours followed by inclusion in a cytotoxicity assay at a ratio of 1:20 (tumor:effector) against PC.3 tumor cells (n=7-13). **e-f,** Box plots of bulk RNA-sequencing transcripts (**e**) and flow cytometry analysis (**f**) of Eomes and T-bet in $CD8^+$ T cells with low or high ΔΨm at activated state (n=6). Statistical significance was determined by Student's Paired (**a**) and non-paired (**b-d, f**) two-tailed t-test, *P<0.05, **P<0.01, ns: not significant.

Extended Data Fig. 3: PD-1/L1 pathway is upregulated in $CD8^+$ T cells with low ΔΨm cells. Hallmark Gene Set Enrichment Analysis (GSEA) of RNA-seq data from three healthy donors was further analyzed with IPA analysis software for pathway regulation. Star indicates the upregulation of PD-1/PD-L1 pathway in low ΔΨm cells.

Fig. 4: Resilient $CD8^+$ T cells have lower glycolytic capacity. a-b, Glycolysis, and glycolytic capacity of sorted $CD8^+$ T cells with low and high ΔΨm after activation with anti-CD3/CD28 beads as measured with extracellular acidification rate (ECAR) analysis and shown with a representative of Seahorse graph (**b,** n=6). **c,** Basal respiration, and spare respiratory capacity of sorted $CD8^+$ T cells with low and high ΔΨm after activation as measured with Mitochondrial Oxygen Consumption Rate (OCR) analysis. **d,** Representative graph of OCR as measured by MitoStress Test (n=6). **e,** OCR/ECAR ratio calculated from the basal respiration values (n=6). **f,** Mitochondrial ATP of activated $CD8^+$ T cells obtained from OCR analysis (n=6). **g,** GLUT1 expression (M (median)FI) in activated $CD8^+$ T cells with low and high ΔΨm (n=4). Statistical significance was determined by Student's paired two-tailed t-test; *P<0.05, ns: not significant.

Fig. 5: Resilient CD8 T cells have lower cytosolic and mitochondrial ROS. a, Hallmark GSEA analysis of reactive oxygen species (ROS) pathway genes from bulk RNA-sequencing

data. **b,** Cytosolic ROS was measured by flow cytometry using CellROX Green and shown as MFI in both resting and activated $CD8^+$ T cells. **c,** Mitochondrial ROS was measured by flow cytometry using MitoSOX over one week in culture media. **d,** Mitochondrial mass was measured using MitoTracker Green with flow cytometry and shown as M (median)FI. **e,** Number of mitochondria per cell was counted via Transmission electron microscopy (TEM) among 10-16 view fields. **f-g,** Cytosolic ROS in $CD8^+$ T cells with low or high ΔΨm were measured from the PBMCs isolated from patients with lung cancer or sarcoma receiving spatially fractionated radiotherapy (SFRT) (**f,** n=9), and from patients with prostate cancer receiving stereotactic body radiotherapy (SBRT) (**g,** n=21). Statistical significance was determined with Student's Non-paired two-tailed t-test; **P<0.01, ***P<0.001, ****P<0.0001, ns: not significant.

Fig. 6: Resilient CD8 T cells express more ME1 to regulate ROS and promote CTL function. a, Volcano plots of bulk RNA-sequencing (RNA-seq) of $CD8^+$ T cells with low or high ΔΨm at resting and activated state (n=3) (ME1 in green circle). **b,** Box plots of ME1 expression analysis with bulk RNA-seq as in (**a**). **c,** Relative ME1 mRNA expression measured with qRT-PCR. **d,** Western blot of ME1 expression as in (**c**) in two donors. **e,** Schematic of functional study of T cells with overexpression of ME1. **f,** ME1 overexpression measured by qRT-PCR in low and high ΔΨm cells. **g, Reactive oxygen species (**ROS) levels (%) measured in $CD8^+$ T cells with low or high ΔΨm isolated from healthy donors (n=3) after transfection with control or ME1 mRNA. **h,** Cytotoxicity assay of $CD8^+$ T cells isolated from healthy donors (n=6) after transfection with control or ME1 mRNA in killing tumor cells (MCF-7) at a ratio of 1:10 of tumor:effector cells. **i,** % $CX3CR1^+$ $NKG7^+$ among $CD8^+$ T cells after transfection with control or ME1 mRNA as measured by flow cytometry (n=4). Statistical significance was determined by Student's Paired two-tailed t-test; *P<0.05, **P<0.01, ns: not significant.

Fig. 7: ME1 increases glycolysis and oxidative phosphorylation, but not ROS, in CD8 T cells. a-b, Seahorse analysis of mitochondrial respiration and ATP production (a) and glycolysis (b) in $CD8^+$ T cells following transfection with control or ME1 mRNA. **c,** Cytosolic **reactive oxygen species (**ROS) in $CD8^+$ T cells following transfection with control or ME1 mRNA as measured by flow cytometry (M (median)FI). **d,** Percent of increased cytotoxicity of PBMCs transfection with ME1 mRNA over PBMCs transfected with control mRNA to normalize different basal level of cytotoxicity of each patient. Cytotoxicity assay was performed at a ratio of 1:10 of tumor:effector cells. **e,** ROS levels (MFI) measured in $CD8^+$ T cells with low or high ΔΨm among PBMCs of patients (n=5) with advanced prostate cancer after transfection with control or ME1 mRNA followed with T cell activation by anti-CD3 antibody for 48 hours. **f,** Graphical illustration of the potential role of ME1 in resilient $CD8^+$ T cells. Statistical significance was determined by Student's Paired (**a, b**) or two-tailed t-test; non-parametric Mann-Whitney correction (**d, e**); *P<0.05, **P<0.01, ns: not significant. CTL = cytotoxic T lymphocytes.

Extended Data Fig. 4: ME1 expression and its regulation of metabolism in $CD8^+$ T cells. a-b, ME1 overexpression measured by Western blot (**a**) followed with quantification of ME1 proteins (**b**) in $CD8^+$ T cells after transfection with control or ME1 mRNA. **c,** Spare respiratory capacity as measured via Seahorse assay. **d**, Reactive oxygen species (ROS) M (median)FI in

resting $CD8^+$ T cells overexpressing ME1 versus control mRNA. Statistical significance was determined by Student's unpaired (**c, d**) two-tailed t-test; non-parametric Mann-Whitney correction, ns: not significant.

METHODS

Specimen collection and T cells isolation

Peripheral blood mononuclear cells (PBMCs) were isolated from healthy donors or patients via centrifugation with lymphoprep (07851, StemCell Technologies) and SepMate conical tubes (85450, StemCell Technologies). $CD8^+$ T cells were then isolated using a magnet based CD8 T cell isolation kit (19053, StemCell Technologies) and used immediately for experiments. Some experiments used PBMCs (patient samples) previously stored in liquid nitrogen. After thawing, PBMCs would be incubated in CTL medium (RPMI 1640 complete medium, rhIL-2: 10 U/ml, rh IL-15: 5 ng/ml; rhIL-7: 5 ng/ml) at 37°C overnight for recovery before transfection.

Patient information. Peripheral blood for this study were collected after written consent was obtained from each participant. Clinical course, treatment information, and outcomes in patients treated with anti-PD-1/L1 therapy and radiation therapy at Mayo Clinic were retrospectively collected. Response to treatment was evaluated according to standard clinical practice guidelines using RECIST [11]. Note that the response listed for anti-PD-1/PD-L1 therapy, (R = complete response, NR = progressive disease, SD = stable disease) was apparent (using RECIST) at the 12-week post-initiation of therapy time-point for all patients. For prostate cancer (receiving SFRT and SBRT), the response was evaluated based on the PSA levels and distance reoccurrence.

Study approval. Peripheral blood for this study from healthy people were acquired from anonymous donors who had consented for blood donation at the Blood Transfusion Center at Mayo Clinic. All donors and patients provided signed informed written consent; the study was approved by the Mayo Clinic Rochester IRB and was conducted according to Declaration of Helsinki principles.

TMRM Staining and Cell Sorting

$CD8^+$ T cells were washed once with 1x PBS and adjusted to a concentration of 1 x 10^6 cells/ml and stained with 0.02 µM final concentration of tetramethylrhodamine methyl ester (TMRM) or 2 nM final concentration of Carbonyl Cyanide 3-chlorophenylhydrazone (CCCP) as control. The TMRM stained cells were incubated at 37°C for 30 minutes with intermittent shaking while the CCCP stained cells were incubated at 37°C for 5 minutes. The cells were then washed twice with 1x PBS and resuspended at 10-15 x 10^6 cells/ml of cell culture media for sorting. The cells were sorted with the BD FACSMelody™ Cell Sorter using the 100-micron sort nozzle and on the PE channel (561nm excitation).

siRNA Transfection

Sorted CD8+ T cells with low and high ΔΨm were centrifuged at 200 x g for 10 minutes prior to nucleofection (4D nucleofector system, Lonza). Three-five million cells were combined with 200 pMol siRNA (siControl or siME1) in 20 µl P3 nucleofection media (Lonza) per well of the 16-well Nucleocuvette strips (X unit). Program FI-115 was used. Following nucleofection, cells were rested in warm RPMI (no FBS, no cytokines) for 4 hours before adding 10% FBS and 10 IU/ml of IL-2, 5 ng/ml of IL-7, and 5 ng/ml of IL-15 into the culture for an overnight recovery followed with subsequent inclusion in experiments.

mRNA Transfection

T cells were transfected with control mRNA or ME1 mRNA (220 µg/ml) using the P3 nucleofection kit (Lonza V4XP-3024) and program FI-115 on the 4D Nucleofector (Lonza). Following nucleofection, cells were rested in warm RPMI (no FBS, no cytokines) for 4 hours before adding 2x CTL medium (as described above) for an overnight recovery followed with T cell activation and functional analysis.

Cytotoxicity Assay

Target tumor cells were washed twice with HBSS, and then labeled with Calcein-AM (5 µM) for 30 minutes and incubation at 37°C in dark, shaking occasionally. The cells were then again washed with HBSS twice and re-suspended at 1 x 10^5/ml in CTL medium with no FBS. Pre-activated $CD8^+$ T cells and target cells were mixed at 1:20 or 1:10 (target to effector ratio) in CTL media without FBS and seeded into 96-U bottom well plate at 200 µl per well. Saponin (0.1%) or Triton X-100 (2%) was added to wells that contained only tumor cells to provide a value for "maximum calcein release," in each assay; tumor cell-only wells were included to measure spontaneous release of calcein. All experimental and control conditions were performed in triplicate wells. The plate was briefly centrifuged at 1,000 rpm for 30 seconds, followed by incubation at 37°C for 4 hours. The plate was then centrifuged at 2,000 rpm for 5 minutes. 100 µl of the 200 µl supernatant was then removed from each well and added to a new, opaque (black) 96 well flat bottom plate (Thermo scientific, 237105). Calcein fluorescence was read using an automated fluorescence measurement system (BioTeK Synergy HTX multi-mode reader) with an excitation of 485/20 and an emission filter of 530/25 scanning for 1 second per well. Percent cytotoxicity was then calculated using the following formula:
% Cytotoxicity = 100 x [(Experimental well release-Spontaneous release well)/Maximum release well-Spontaneous release well].

Degranulation assay

T cells were adjusted at a concentration of 1 x 10^6 cells/100 µl CTL medium including Golgi-Stop (Biolegend, 420701) and Golgi-Plug (Biolegend, 420601) and incubated with 5 µl of CD107a antibody (Biolegend, H4A3) and 5 µl of anti-CD3/CD28 beads. The cells were then briefly centrifuged at 300 x g for 1 minute and incubated at 37°C for 5 hours. After the incubation, the cells were stained with TMRM followed with surface antibody staining before flow cytometry analysis.

ROS detection

Cells were stained with 250 nM of CellROX (ThermoFisher Scientific, C10492 or 1 µM of MitoSOX (ThermoFisher Scientific, M36008) in complete media and incubated at 37°C for 45 minutes. From there, the cells were resuspended in FACS buffer (1x PBS, 2mM EDTA, and 3% FBS) at a concentration of 1 x 10^6 cells/ 100 µl followed by staining with antibodies for surface molecules for 20 minutes at room temperature in the dark. Cells were then washed once in FACS buffer, resuspended in 200 µl, and analyzed on Bio-Rad ZE5 Cell Analyzer. Analysis was performed using FlowJo V10.

Flow Cytometry Analysis

Cells were adjusted to 0.5-1 x 10^6 cells/ml with 1x PBS and stained with live/dead dye and incubated at 4°C for 30 minutes. The cells were then washed once with 1x PBS followed by staining for cell surface molecules. For intracellular molecule staining, cells were incubated with FoxP3 Fixation Buffer overnight at 4ºC. After fixation, cells were washed once with 1x permeabilization buffer, and then stained with antibodies for intracellular molecules such as ME1, TCF-1/7, TOX, Eomes, T-bet, Ki67, HIF1-α, NKG7, and Glut1 for 1 hour at 4ºC in 100 µl of 1x permeabilization buffer. Following intracellular staining, cells were washed once with 1x permeabilization buffer and then resuspended in 200 µl FACS buffer for flow cytometry analysis, which was completed on a Cytoflex LX (Beckman Coulter) (DAQ Version V2.233, MCB Version: V3.01) running CytExpert software. Flow cytometric analysis was performed using FlowJo V10.

Quantitative PCR

RNA was isolated using Qiagen RNeasy Plus Mini Kit (74134, Qiagen). RT-reaction was completed using SuperScript™ III Reverse Transcriptase (18080-400, Invitrogen). qRT-PCR analysis was completed using a Quant-Studio 3 Real-Time PCR System (Applied Biosystems) and TaqMan Fast Advanced Master Mix (444455, Applied Biosystems). Taqman assays included: Hs01120688-gl, Human ME1-FAM and Hs99999901-Sl, Human-18s-FAM, both from Applied Biosystems. All samples were run in doublet. Relative expression was calculated using the $2^{-\Delta Ct}$ method. Granzyme B (F 5-TACCATTGAGTTGTGCGTGGG-3, R 5-GCCATTGTTTCGTCCATAGGAGA-3, ME1 (F 5-GGGAGACCTTGGCTGTAATGG-3, R 5-TTCGGTTCCCACATCCAGAAT-3), UBE (F 5-GTACTCTTGTCCATCTGTTCTCTG-3; R 5-CCATTCCCGAGCTATTCTGTT-3). RNA input was normalized to 20 ng/ul with 10 ul input for the RT reaction. Post RT reaction cDNA was diluted 1:5 before amplification on the Quantstudio 3 in the following volume per well: 5 µl cDNA template, 10 µl SYBR green (Applied Biosystems), 3 µl H_2O, 1 µl 10 mM Forward/Reverse primer.

Western Blots

Cell pellets were lysed in NP-40 buffer and concentrations measured via protein assay using BioRad reagent (#500-0006). Once diluted to equal concentrations, samples were combined with Laemmli sample buffer (BioRad) with beta-mercaptoethanol and run using a Mini-PROTEAN Electrophoresis and Transfer system (BioRad). Membranes were incubated with primary antibody overnight at 4°C (ME1, Beta-Actin, or GAPDH). Secondary antibodies were added the

next morning for 2 hours (HRP-conjugated anti-mouse). Signal was visualized using SuperSignal West Pico PLUS Chemiluminescence Substrate Kit (34577, Thermo Fisher) on a Syngene G: Box Chemi XX6 system running GeneSys software (V1.6.1.0). Full images of all membranes are included in the supplementary source data files.

Transmission electron microscopy (TEM) analysis of mitochondria

Cells were fixed in Trump fixative for 1 hour at room temperature or at 4ºC overnight followed with a fixation for 1 hour in 1% osmium tetroxide. The samples were dehydrated, embedded in Spurrs resin, sectioned at 90 nm, and observed using a Joel 1400 electron microscope (Joel USA Inc.). For quantification, images of individual T cell in a single field of view downloaded into JPEG images and the number of mitochondria structures within the T cells were counted manually by two different readers.

Metabolic Assays

Seahorse Xfe96 Bioanalyzer (Agilent) was used to determine OCR and ECAR. Sorted cells or total $CD8^+$ T cells were washed in XF Base media (Seahorse XF RPMI medium with 2 mM glutamine, 10 mM glucose, 1 mM sodium pyruvate, and 5 mM HEPES (4-(2-hydroxyethyl)-1-piperazineethanesulfonic acid), pH 7.4 at 37 °C) for OCR or XF media with 2 mM glutamine for ECAR before being plated onto Seahorse cell culture plates coated with Cell-Tak (Corning #354240) at 1×10^5 cells per well. The cells were allowed to adhere to culture plate. The OCR was measured via Seahorse Mito Stress assay (Agilent), with addition of oligomycin (2 μM), carbonyl cyanide 4-(trifluoromethoxy) phenylhydrazone (FCCP; 1.2 μM) and Rotenone and Antimycin (1.0 μM)). The ECAR was measured with addition of 10 mM glucose, 2 μM oligomycin, and 50 nM 2-deoxy-D-glucose (2-DG). Assay parameters were as follows: 3-minute mix, no wait, 3-minute measurement, repeated 3–4 times at basal and after each addition. SRC was calculated as oxygen consumption rate (OCR) at maximum rate (OCR_{Max}) − OCR in basal state (OCR_{Bas}). Mitochondrial ATP production was calculated by subtracting the minimum respiration rate after oligomycin injection from the basal respiration rate before oligomycin injection.

Mitochondria mass Staining

Cells at a concentration of 1×10^6 cell/ml were washed once with 1x PBS and incubated with 100 nM of MitoTracker Green FM dye for 30 minutes at 37 °C. The cells were then analyzed by flow cytometry.

Bulk RNA sequencing

RNA was isolated using Qiagen Rneasy Plus Mini Kit (74134, Qiagen). The bulk RNA paired-end sequencing reads were processed through the Mayo bioinformatics pipelines MAP-Rseq (v3.0) as we previously reported. Reads were aligned to human reference genomes (hg38). The RNA aligned reads were quantified for gene expression using the Subread package. Differences across groups were assessed using bioinformatics package edgeR 2.6.2 to identify differentially expressed genes. Such genes were reported with magnitude of change (log2 scale) and their level

of significance (False Discovery Rate, FDR < 5%). For pathway analysis, T cells with low or high ΔΨm were randomized and put through Gene Set Enrichment Analysis (GSEA) as described in the user guide.

Statistical Analyses

Data were analyzed in GraphPad Prism (version 9) using the unpaired or paired, two-tailed *t*-test without correction for multiple comparisons, as indicated in figure legends.

Antibody List

Target	Host	Clone	Flour	Company	Catalogue #	Final conc./dilution
Human CX3CR1 Human CX3CR1	Rat Rat	2A9-1 2A9-1	APC-Cy7 BV-510	Biolegend Biolegend	341616 341622	Flow @1:20 Flow @1:20
Human Granzyme B	Mouse	CLB-GB11	PERCP	Novus	NBP1-50071PCP	Flow @1:100
Human PD1 Human PD-1 Human PD-1	Mouse Mouse Mouse	EH12.2H7 EH12.2H7 EH12.1	APC APC-Cy7 BV510	Biolegend Biolegend BD Horizon	329908 329922 563076	Flow @1:20 Flow @1:20 Flow @1:20
Human TCF-1 Human TCF-1	Rabbit Rabbit	C63D9 C63D9	Pac-Blue PE	Cell Signaling Cell Signaling	#9066 #14456	Flow @1:50 Flow @1:50
Human EOMES	Mouse	WD1928	FITC	eBioscience by ThermoFisher	11-4877-42	Flow @1:20
Human TOX	Recombinant	REA473	PE	Miltenyi Biotec	130-120-716	Flow @1:50
Human Tbet	Mouse	4B10	APC	Biolegend	644814	Flow @1:20
Human HIF-1α	Mouse	Mgc3	APC	eBioscience by ThermoFisher	17-7528-82	Flow @1:20
Human GLUT1	Mouse	202915	FITC	R&D Systems	FAB1418F	Flow @1:20
Human CCR7 Human CCR7	Mouse Mouse	2-L1-A G043H7	BV 650 FITC	BD Horizon Biolegend	566756 353216	Flow @1:20 Flow @1:20
Human CD45RA Human CD45RA Human CD45RA	Mouse Mouse Mouse	HI100 HI100 5H9	BV 510 APC BUV496	BD Horizon eBioscience by ThermoFisher Biolegend	563031 17-0458-42 741182	Flow @1:20 Flow @1:20 Flow @1:20
Human Ki67	Mouse	Ki-67	APC	Biolegend	350514	Flow @1:20
Human CD8 Human CD8	Mouse Mouse	RPA-T8 SK1	PE-Cy7 BV 510	BD Horizon Biolegend	557746 344732	Flow @1:20 Flow @1:20

Human CD8	Mouse	SK1	APC	Biolegend	344722	Flow @1:20
Human CD3 Human CD3 Human CD3	Mouse Mouse Mouse	UCHT1 UCHT1 OKT3	BV 650 PECy5.5 BV 421	Biolegend Biolegend Biolegend	300468 300410 317344	Flow @1:20 Flow @1:20 Flow @1:20
Human CD11a Human CD11a Human CD11a	Mouse Mouse Mouse	TS2/4 HI111 HI111	PerCP/Cy5.5 PE-Cy7 APC-Cy7	Biolegend Biolegend Biolegend	350614 301220 301236	Flow @1:20 Flow @1:20 Flow @1:20
Human ME1 Human ME1	Mouse Mouse		None PE	Santa Cruz Biotechnology	sc-365891 sc-365891	Western Blot @ 1:1000 Flow @1:50
Human CD107a	Mouse	H4A3	FITC	Biolegend	328606	Flow @1:20
Brefeldin A				Biolegend	420601	
Monensin				Biolegend	420701	
Mouse IgG	Mouse	Polyclonal	None			
Rabbit IgG	Rabbit	Polyclonal	None			
Peroxidase affiniPure Donkey anti-mouse IgG (H+L)		Polyclonal		Jackson ImmunoResearch	715-035-151	Western blot @ 1:5000
Beta-actin	Rabbit		None	Cell Signaling	#4970S	Western blot @ 1:2000

Dyes

Reagent (Fluoro)	**Supplier**	**Catalogue #**	**Final conc.**
Ghost Dye UV 450 (UV405)	Tonbo biosciences	13-0868-T100	Flow @1:100
Ghost Dye V 450 (BV450)	Tonbo biosciences	13-0863-T100	Flow @1:100
CellROX Green Flow Kit	ThermoFisher Scientific	C10492	Flow @500nM/mL
MitoSOX Red	ThermoFisher Scientific	M36008	Flow @100nM/mL
MitoTracker Green FM	ThermoFisher Scientific	M7514	Flow @100nM/mL
CellTrace™ CFSE dye	ThermoFisher Scientific	C34554	Flow @ 2.5µM/mL
TMRM, perchlorate	Biotium	70017	Flow @0.02µM
TMRM	ThermoFisher Scientific	M20036	Flow @0.02µM

CD8+ isolation and nucleofection reagents

Reagent	**Supplier**	**Catalogue #**
Lymphoprep	StemCell Technologies	07851
SepMate Conical tubes	StemCell Technologies	85450
EasySep Human $CD8^+$ T cell Isolation Kit	StemCell Technologies	Q-263176

P3 Primary Cell 4D-Nucleofector X Kit S	Lonza	V4XP-3032
P3 Primary Cell 4D-Nucleofector X Kit L	Lonza	V4XP-3024

qPCR reagents

Reagent	Supplier	Catalogue #
RLT buffer	Qiagen	79216
Qiagen RNeasy Plus Mini Kit	Qiagen	74134
SuperScript™ III Reverse Transcriptase	ThermoFisher Scientific	18080-400
TaqMan Fast Advanced Master Mix	Applied Biosystems	444455

Seahorse reagents

Reagent	Supplier	Catalogue #
Seahorse XF Cell Mito Stress Test Kit	Agilent	103015-100
Seahorse XF Glycolysis Stress Test Kit	Agilent	103020-100
Seahorse XFe96 FluxPak mini	Agilent	102601-100
Seahorse XF Cell Energy Phenotype Test Kit	Agilent	103325-100
Seahorse XF RPMI medium pH 7.4, 500mL	Agilent	103576-100
Seahorse XF 100mM pyruvate solution, 50mL	Agilent	103578-100
Seahorse XF 200mM glutamine solution, 50mL	Agilent	103579-100
Seahorse XF 1.0 M glucose solution, 50mL	Agilent	103577-100
Corning Cell-Tak Cell and Tissue Adhesive, 1 mg	Corning	354240

Inhibitors

Reagent	Supplier	Catalogue #	Final conc.
Oligomycin (OCR)	Agilent	103015-100	2.0µM
FCCP	Agilent	103015-100	1.5µM
Rot/AA	Agilent	103015-100	1.0µM
Glucose	Agilent	103020-100	10mM
Oligomycin (ECAR)	Agilent	103020-100	2.0µM
2-DG	Agilent	103020-100	50nM

Primer List

Primer	Sequence	Usage Notes
Human Full Length ME1 F	GGGAGACCTTGGCTGTAATGG	
Human Full Length ME1 R	TTCGGTTCCCACATCCAGAAT	
Human Full Length GZMB F	TACCATTGAGTTGTGCGTGGG	
Human Full Length GZMB R	GCCATTGTTTCGTCCATAGGAGA	
Human Full Length UBE F	GTACTCTTGTCCATCTGTTCTCTG	

Human Full Length UBE R	CCATTCCCGAGCTATTCTGTT	

KD and mRNA Overexpression reagents:

Reagent	Company/Catalogue or sequence	Catalogue #	Usage Notes
ME1 siRNA SMARTpool: ON-TARGETplus	Dharmacon	L-009348-00-0020	
Control siRNA ON-TARGETplus Non-targeting pool	Dharmacon	D-001810-10-20	
ME1 mRNA for human studies	TriLink Biotechnologies	L-7007	
Control mRNA	TriLink Biotechnologies	L-7610	

Cell culture reagents:

Reagent	Company	Catalogue #	Final conc/Usage Notes
DMEM	Gibco	11885-084	Base media for MCF-7
RPMI	Corning	10-040-CV	Base media for PC.3
HEPES buffer	Corning	25-060-CI	Added 10 mL of the 1M solution to 500 mL of all cell culture media
FBS	Gibco	10437-028	Final concentration of 10% FBS used for all cell culture media
FoxP3/TF Fixation/Permeabilization concentrate and diluent	eBioscience by ThermoFisher	00-5521-00	
Pen/Strep	Cellgro	30-002-CI	Used 5mL of the 100X solution in 500 mL of all cell culture media
Recombinant human IL-2	Peprotech	200-02	10U/ml unless otherwise stated in methods.
Recombinant human IL-15	Peprotech	200-15	10ng/mL
Recombinant human IL-7	Peprotech	200-07	10ng/mL

Purified NA/LE Mouse Anti-human CD3 (Clone HIT3a)	BD Horizon	555336	
Purified NA/LE Mouse anti-human CD28 (Clone CD28.2)	BD Horizon	555725	

Acknowledgements
We thank all the patients who generously contributed samples and participated in the study. We thank all members of the Dong laboratory for helpful discussions and critical analysis of the manuscript. We also acknowledge the Department of Radiation Oncology and Division of Medical Oncology at the Mayo Clinic for providing excellent patient care. This study was supported in part by the generosity of Mayo Clinic benefactors. We acknowledge the Genome Analysis Core at Mayo Clinic, including technologists Vernadette A. Simon and Fariborz Rakhshan-Rohakhtar as well as supervisors Julie S. Lau, Samantha J. McDonough, and Mark Mutawe. We are grateful for the electron microscopy imaging service provided by Bing Huang and Scott I. Gamb; and Flow cytometry and Sorting services provided by Holly Lamb, Colleen Moe, Han Yong Hwan, and Drew Kluge at the Mayo Clinic Microscope and Cell Analysis Core. The staff at Mayo Clinic Blood transfusion center. BioRender was used to create the graphics throughout the manuscript. We acknowledge support from the Mayo Clinic Center for Individualized Medicine's IMPRESS program and High-Definition Therapeutics program (H. Dong), the Mayo Clinic Center for Biomedical Discovery (H. Dong), the Mayo Clinic Cancer Center's David F. and Margaret T. Grohne Cancer Immunology and Immunotherapy program (H. Dong), NIH grant R21 CA251923 (A.S. Mansfield), NIH grant K12 CA 090628 (Y. Yan), NIH grant R01 AR077518 (Hu Zeng), NIH grant R21 CA197878 (H. Dong), NIH grant R01 AI095239 (H. Dong), NIH grant R01 CA200551 (H. Dong and S.S. Park), NIH grant R01 CA256927 (H. Dong), and NIH grant R01 200551 (S.S. Park and H. Dong). This project is partially funded by the Lawrence and Marilyn Matteson Award S.S. Park, D.O, and M.P. Grams), and Sydney Luckman Family Predoctoral Award (J.K.G).

Author contributions
J.K.G. and H.D. conceived the project, designed experiments, and wrote the manuscript. J.K.G. performed most of the experiments. Z.M., C.L., J.B.H., V.V.V., E.R.D., M.A.H., W.B., and Y.H. processed patient blood samples, conducted some of the flow cytometry experiments, Western blot experiments and qRT-PCR. Y.L (Li). analyzed the bulk RNAseq data and J.K.G. ran the GSEA analysis. G.D. performed healthy donors' ME1 overexpression cytotoxicity assays and Western blots. F.A., S.H., and J.J.O. performed statistical analysis. F.L. and H.Z. advised on biochemical and metabolic assays and provided critical edits to the manuscript. X.W. provided guidance on messenger RNA design and construct. Y.Y., R.X.D., M.Z., S.N.M., A.S.M., Y.L.(Lin)., M. G., D.O. and S.S.P. provided clinical samples and interpretation of clinical data. All authors reviewed the manuscript.

References

1. Walsh, S.R., *et al.* Endogenous T cells prevent tumor immune escape following adoptive T cell therapy. *The Journal of clinical investigation* **129**, 5400-5410 (2019).
2. Evans, J.D., *et al.* Prospective Immunophenotyping of CD8(+) T Cells and Associated Clinical Outcomes of Patients With Oligometastatic Prostate Cancer Treated With Metastasis-Directed SBRT. *Int J Radiat Oncol Biol Phys* **103**, 229-240 (2019).
3. Zhang, H., *et al.* Phase II Evaluation of Stereotactic Ablative Radiotherapy (SABR) and Immunity in (11)C-Choline-PET/CT-Identified Oligometastatic Castration-Resistant Prostate Cancer. *Clin Cancer Res* **27**, 6376-6383 (2021).
4. Yan, Y., *et al.* CX3CR1 identifies PD-1 therapy-responsive CD8+ T cells that withstand chemotherapy during cancer chemoimmunotherapy. *JCI Insight* **3**(2018).
5. Gicobi, J.K., Barham, W. & Dong, H. Immune resilience in response to cancer therapy. *Cancer Immunology, Immunotherapy* **69**, 2165-2167 (2020).
6. Gicobi, J.K., Dellacecca, E.R. & Dong, H. Resilient T-cell responses in patients with advanced cancers. *Int J Hematol* (2022).
7. Zhang, Y., *et al.* A T cell resilience model associated with response to immunotherapy in multiple tumor types. *Nat Med*, 1421–1431 (2022).
8. An, H.J., Chon, H.J. & Kim, C. Peripheral Blood-Based Biomarkers for Immune Checkpoint Inhibitors. *Int J Mol Sci* **22**, 9414 (2021).
9. Sade-Feldman, M., *et al.* Defining T Cell States Associated with Response to Checkpoint Immunotherapy in Melanoma. *Cell* **175**, 998-1013.e1020 (2018).
10. Wu, T.D., *et al.* Peripheral T cell expansion predicts tumour infiltration and clinical response. *Nature* **579**, 274-278 (2020).
11. Yan, Y., *et al.* CX3CR1 identifies PD-1 therapy-responsive CD8+ T cells that withstand chemotherapy during cancer chemoimmunotherapy. *JCI Insight* **3**, e97828 (2018).
12. Yost, K.E., *et al.* Clonal replacement of tumor-specific T cells following PD-1 blockade. *Nat Med* **25**, 1251-1259 (2019).
13. Yamauchi, T., *et al.* T-cell CX3CR1 expression as a dynamic blood-based biomarker of response to immune checkpoint inhibitors. *Nat Commun* **12**, 1402 (2021).
14. Zander, R., *et al.* CD4(+) T Cell Help Is Required for the Formation of a Cytolytic CD8(+) T Cell Subset that Protects against Chronic Infection and Cancer. *Immunity* **51**, 1028-1042.e1024 (2019).
15. Griffin, R.J., *et al.* Understanding High-Dose, Ultra-High Dose Rate, and Spatially Fractionated Radiation Therapy. *Int J Radiat Oncol Biol Phys* **107**, 766-778 (2020).
16. Grams, M.P., *et al.* VMAT Grid Therapy: A Widely Applicable Planning Approach. *Pract Radiat Oncol* **11**, e339-e347 (2021).
17. Li, C., *et al.* A high OXPHOS CD8 T cell subset is predictive of immunotherapy resistance in melanoma patients. *J Exp Med* **219**, e20202084 (2022).
18. Li, C., *et al.* The Transcription Factor Bhlhe40 Programs Mitochondrial Regulation of Resident CD8(+) T Cell Fitness and Functionality. *Immunity* **51**, 491-507.e497 (2019).
19. Nishida, M., *et al.* Mitochondrial reactive oxygen species trigger metformin-dependent antitumor immunity via activation of Nrf2/mTORC1/p62 axis in tumor-infiltrating CD8T lymphocytes. *J Immunother Cancer* **9**, e002954 (2021).
20. Ogando, J., *et al.* PD-1 signaling affects cristae morphology and leads to mitochondrial dysfunction in human CD8(+) T lymphocytes. *J Immunother Cancer* **7**, 151 (2019).

21. Simula, L., *et al.* PD-1-induced T cell exhaustion is controlled by a Drp1-dependent mechanism. *Mol Oncol* **16**, 188-205 (2022).
22. Yu, Y.-R., *et al.* Disturbed mitochondrial dynamics in CD8+ TILs reinforce T cell exhaustion. *Nature Immunology* **21**, 1540-1551 (2020).
23. Sukumar, M., *et al.* Mitochondrial Membrane Potential Identifies Cells with Enhanced Stemness for Cellular Therapy. *Cell Metab* **23**, 63-76 (2016).
24. Khan, O., *et al.* TOX transcriptionally and epigenetically programs CD8(+) T cell exhaustion. *Nature* **571**, 211-218 (2019).
25. Buggert, M., *et al.* T-bet and Eomes are differentially linked to the exhausted phenotype of CD8+ T cells in HIV infection. *PLoS Pathog* **10**, e1004251 (2014).
26. Intlekofer, A.M., *et al.* Effector and memory CD8+ T cell fate coupled by T-bet and eomesodermin. *Nat Immunol* **6**, 1236-1244 (2005).
27. Pearce, E.L., *et al.* Control of effector CD8+ T cell function by the transcription factor Eomesodermin. *Science* **302**, 1041-1043 (2003).
28. Szabo, S.J., *et al.* A novel transcription factor, T-bet, directs Th1 lineage commitment. *Cell* **100**, 655-669 (2000).
29. Llaó-Cid, L., *et al.* EOMES is essential for antitumor activity of CD8(+) T cells in chronic lymphocytic leukemia. *Leukemia*, 3152–3162 (2021).
30. Raveney, B.J.E., *et al.* Involvement of cytotoxic Eomes-expressing CD4⁺ T cells in secondary progressive multiple sclerosis. *Proceedings of the National Academy of Sciences* **118**, e2021818118 (2021).
31. Amitrano, A.M., *et al.* Optical Control of CD8(+) T Cell Metabolism and Effector Functions. *Front Immunol* **12**, 666231 (2021).
32. Maciolek, J.A., Pasternak, J.A. & Wilson, H.L. Metabolism of activated T lymphocytes. *Curr Opin Immunol* **27**, 60-74 (2014).
33. Newsholme, E.A., Crabtree, B. & Ardawi, M.S. The role of high rates of glycolysis and glutamine utilization in rapidly dividing cells. *Biosci Rep* **5**, 393-400 (1985).
34. Finlay, D. & Cantrell, D.A. Metabolism, migration and memory in cytotoxic T cells. *Nat Rev Immunol* **11**, 109-117 (2011).
35. Ma, E.H., *et al.* Metabolic Profiling Using Stable Isotope Tracing Reveals Distinct Patterns of Glucose Utilization by Physiologically Activated CD8(+) T Cells. *Immunity* **51**, 856-870 e855 (2019).
36. Vander Heiden, M.G., Cantley, L.C. & Thompson, C.B. Understanding the Warburg effect: the metabolic requirements of cell proliferation. *Science* **324**, 1029-1033 (2009).
37. Dan, L., *et al.* The phosphatase PAC1 acts as a T cell suppressor and attenuates host antitumor immunity. *Nature Immunology* **21**, 287-297 (2020).
38. Scharping, N.E., *et al.* Mitochondrial stress induced by continuous stimulation under hypoxia rapidly drives T cell exhaustion. *Nature Immunology* **22**, 205-215 (2021).
39. Simmen, F.A., Alhallak, I. & Simmen, R.C.M. Malic enzyme 1 (ME1) in the biology of cancer: it is not just intermediary metabolism. *J Mol Endocrinol* **65**, R77-R90 (2020).
40. Lu, Y.X., *et al.* ME1 Regulates NADPH Homeostasis to Promote Gastric Cancer Growth and Metastasis. *Cancer Res* **78**, 1972-1985 (2018).
41. Sena, L.A., *et al.* Mitochondria are required for antigen-specific T cell activation through reactive oxygen species signaling. *Immunity* **38**, 225-236 (2013).
42. Wen, T., *et al.* NKG7 Is a T-cell-Intrinsic Therapeutic Target for Improving Antitumor Cytotoxicity and Cancer Immunotherapy. *Cancer Immunol Res* **10**, 162-181 (2022).

43. Liu, C.*, et al.* Malic Enzyme 1 Indicates Worse Prognosis in Breast Cancer and Promotes Metastasis by Manipulating Reactive Oxygen Species. *Onco Targets Ther* **13**, 8735-8747 (2020).
44. Gorrini, C., Harris, I.S. & Mak, T.W. Modulation of oxidative stress as an anticancer strategy. *Nat Rev Drug Discov* **12**, 931-947 (2013).
45. Meermeier, E.W.*, et al.* Tumor burden limits bispecific antibody efficacy through T cell exhaustion averted by concurrent cytotoxic therapy. *Blood Cancer Discov* **2**, 354-369 (2021).
46. Zheng, L.*, et al.* Pan-cancer single-cell landscape of tumor-infiltrating T cells. *Science* **374**, abe6474 (2021).
47. Fang, X.*, et al.* TCF-1(+) PD-1(+) CD8(+)T cells are associated with the response to PD-1 blockade in non-small cell lung cancer patients. *J Cancer Res Clin Oncol*, 2653–2660 (2021).
48. Hudson, W.H.*, et al.* Proliferating Transitory T Cells with an Effector-like Transcriptional Signature Emerge from PD-1(+) Stem-like CD8(+) T Cells during Chronic Infection. *Immunity* **51**, 1043-1058.e1044 (2019).
49. Jansen, C.S.*, et al.* An intra-tumoral niche maintains and differentiates stem-like CD8 T cells. *Nature* **576**, 465-470 (2019).
50. Siddiqui, I.*, et al.* Intratumoral Tcf1⁺PD-1⁺CD8⁺ T Cells with Stem-like Properties Promote Tumor Control in Response to Vaccination and Checkpoint Blockade Immunotherapy. *Immunity* **50**, 195-211.e110 (2019).
51. Wen, S.*, et al.* TCF-1 maintains CD8(+) T cell stemness in tumor microenvironment. *J Leukoc Biol* **110**, 585-590 (2021).
52. Zhang, J., Lyu, T., Cao, Y. & Feng, H. Role of TCF-1 in differentiation, exhaustion, and memory of CD8(+) T cells: A review. *Faseb j* **35**, e21549 (2021).

Figures

Fig.1

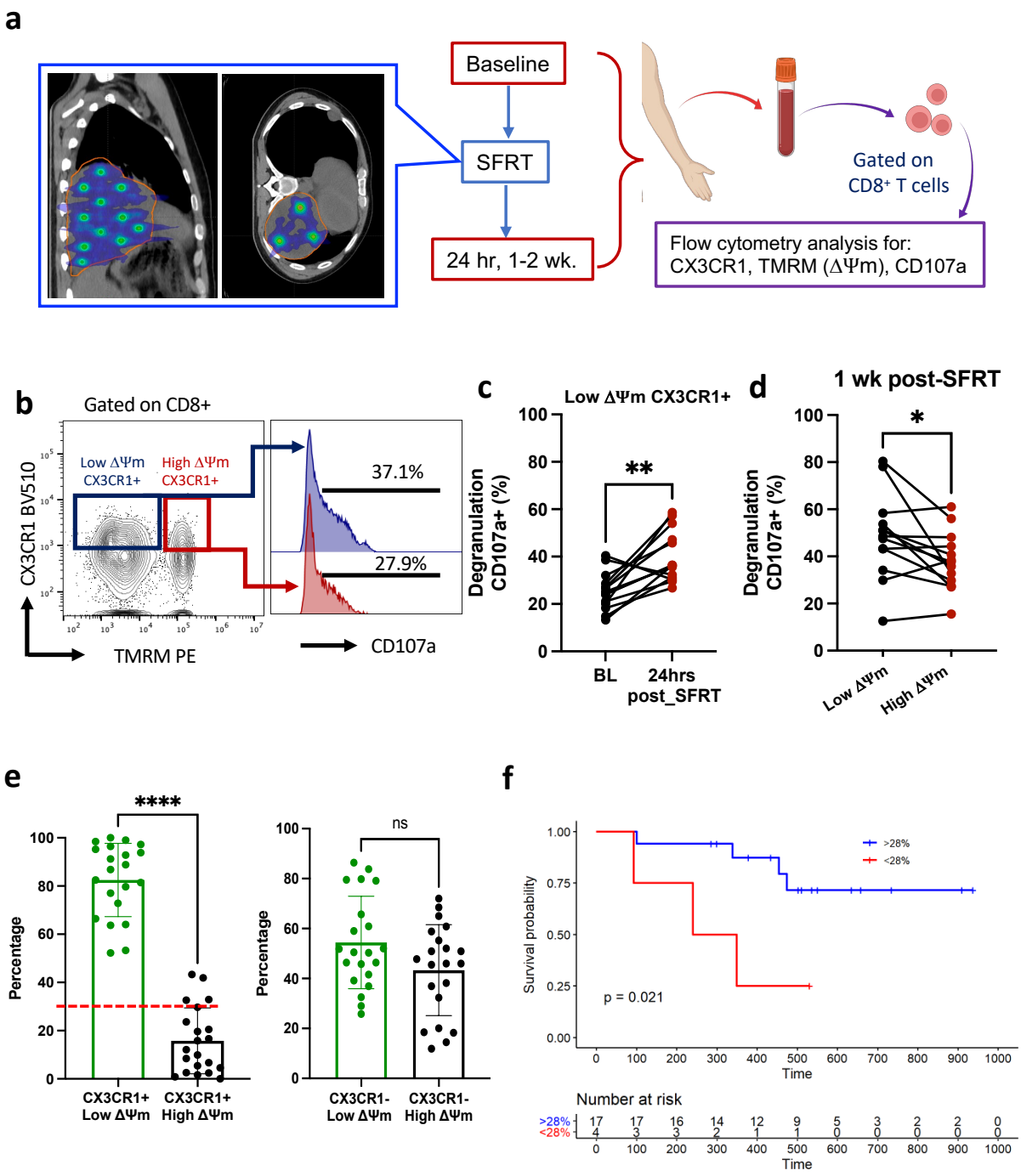

Extended data Fig. 1

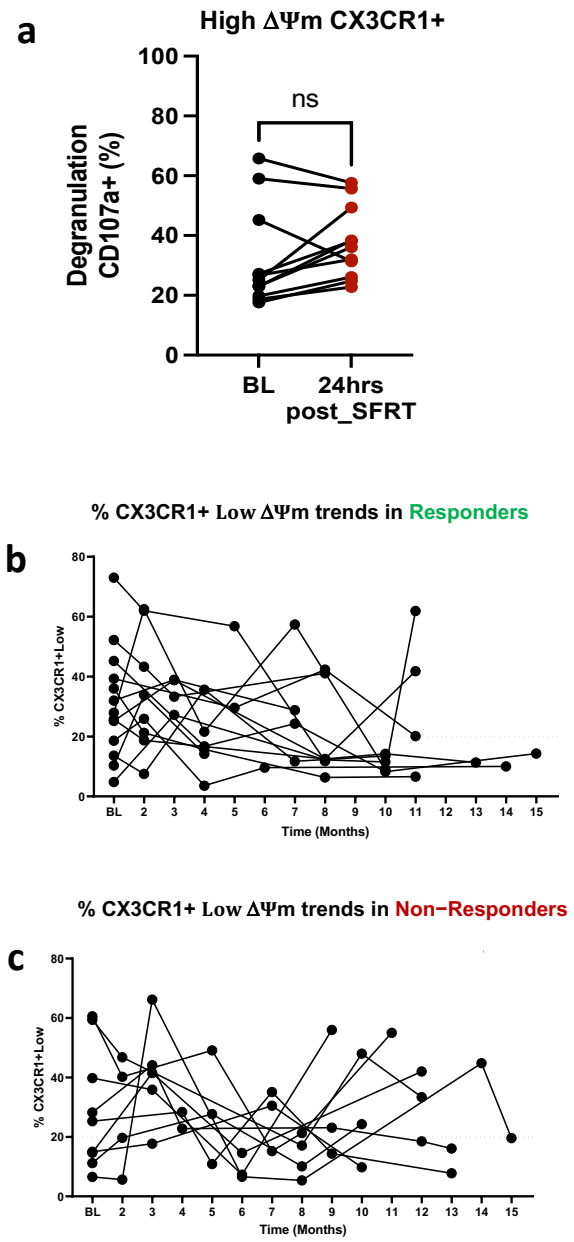

Fig. 2

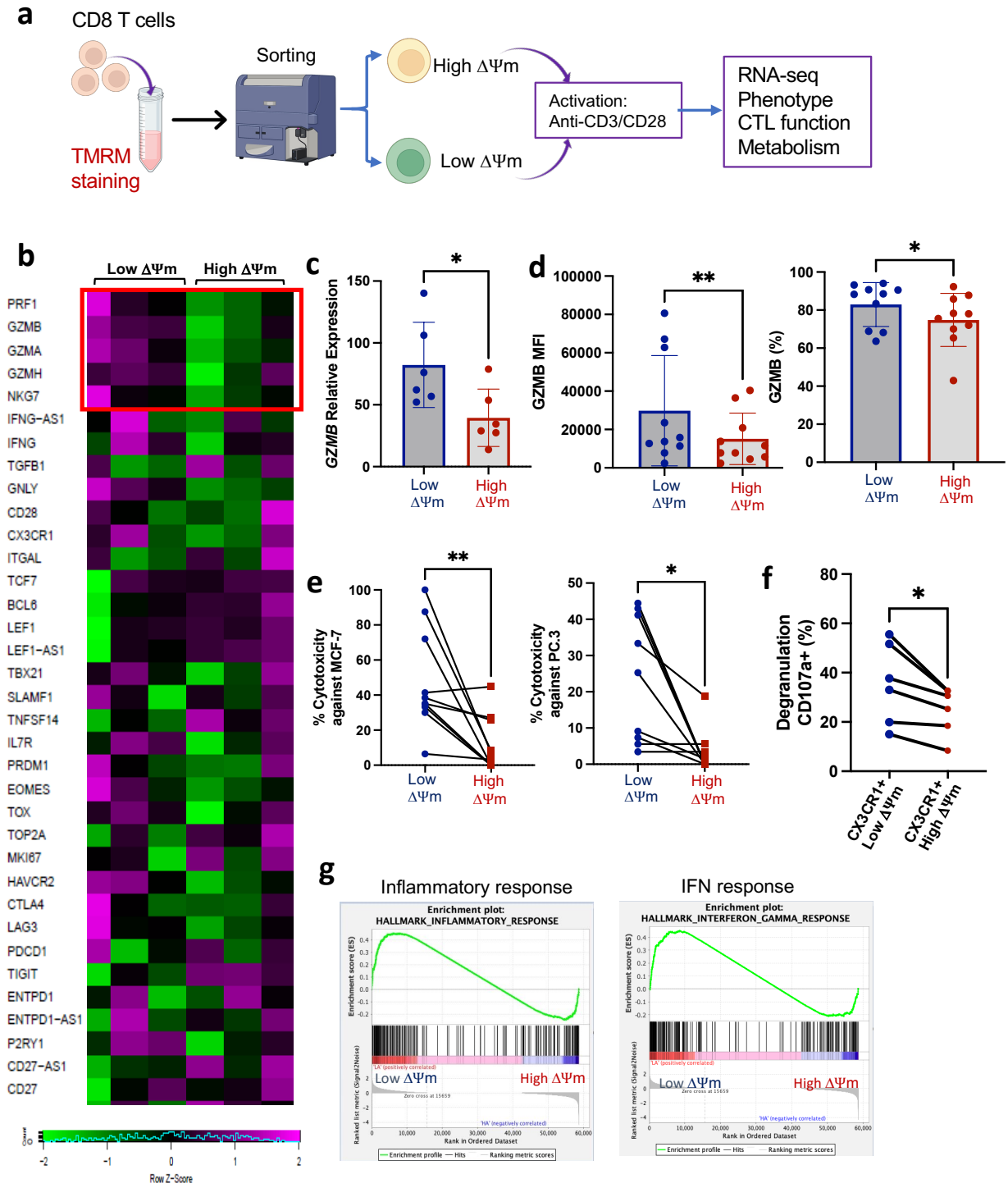
a
CD8 T cells
TMRM staining
Sorting
High ΔΨm
Low ΔΨm
Activation: Anti-CD3/CD28
RNA-seq
Phenotype
CTL function
Metabolism
b
Low ΔΨm
High ΔΨm
PRF1
GZMB
GZMA
GZMH
NKG7
IFNG-AS1
IFNG
TGFB1
GNLY
CD28
CX3CR1
ITGAL
TCF7
BCL6
LEF1
LEF1-AS1
TBX21
SLAMF1
TNFSF14
IL7R
PRDM1
EOMES
TOX
TOP2A
MKI67
HAVCR2
CTLA4
LAG3
PDCD1
TIGIT
ENTPD1
ENTPD1-AS1
P2RY1
CD27-AS1
CD27
Row Z-Score
c
GZMB Relative Expression
d
GZMB MFI
GZMB (%)
e
% Cytotoxicity against MCF-7
% Cytotoxicity against PC.3
f
Degranulation CD107a+ (%)
CX3CR1+ Low ΔΨm
CX3CR1+ High ΔΨm
g
Inflammatory response
IFN response
Enrichment plot: HALLMARK_INFLAMMATORY_RESPONSE
Enrichment plot: HALLMARK_INTERFERON_GAMMA_RESPONSE
Low ΔΨm
High ΔΨm
Rank in Ordered Dataset

Extended data Fig. 2

a

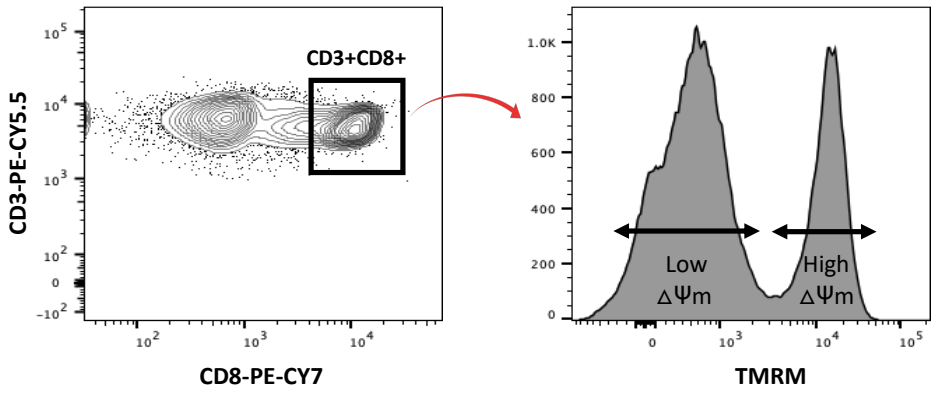

b

IL-2 STAT5 signaling

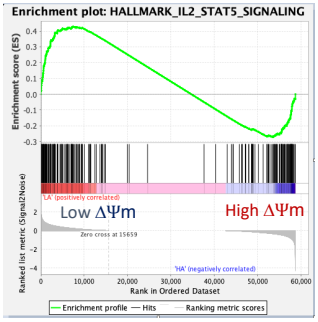

c

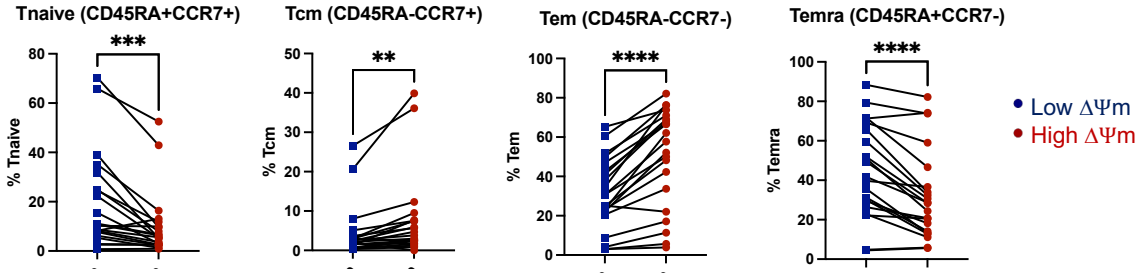

Fig. 3

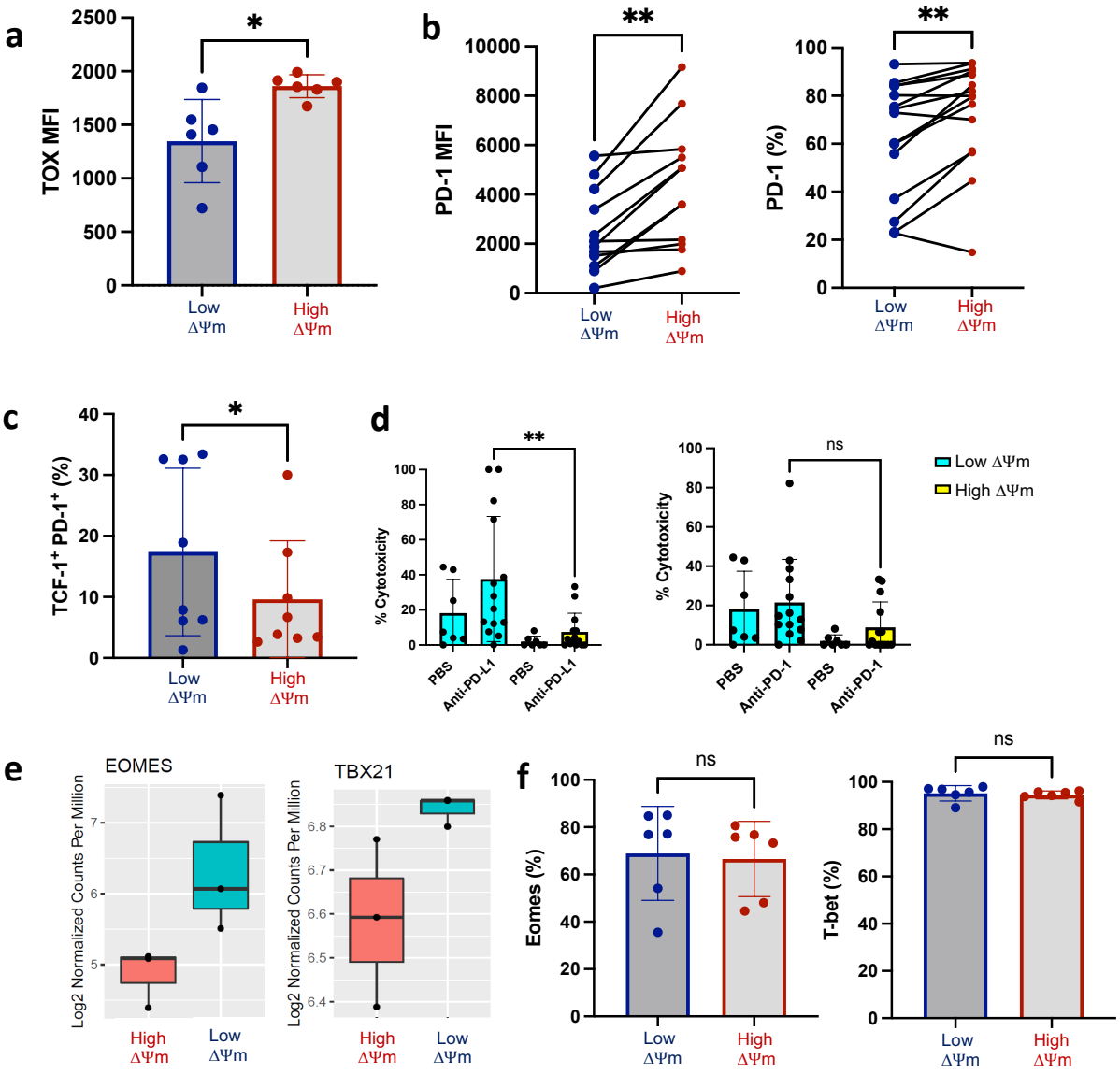
a
TOX MFI
2500
2000
1500
1000
500
0
*
Low ΔΨm
High ΔΨm
b
PD-1 MFI
10000
8000
6000
4000
2000
0
**
Low ΔΨm
High ΔΨm
PD-1 (%)
100
80
60
40
20
0
**
Low ΔΨm
High ΔΨm
c
TCF-1+ PD-1+ (%)
40
30
20
10
0
*
Low ΔΨm
High ΔΨm
d
% Cytotoxicity
100
80
60
40
20
0
**
PBS
Anti-PD-L1
PBS
Anti-PD-L1
% Cytotoxicity
100
80
60
40
20
0
ns
PBS
Anti-PD-1
PBS
Anti-PD-1
Low ΔΨm
High ΔΨm
e
EOMES
Log2 Normalized Counts Per Million
7
6
5
High ΔΨm
Low ΔΨm
TBX21
Log2 Normalized Counts Per Million
6.8
6.7
6.6
6.5
6.4
High ΔΨm
Low ΔΨm
f
Eomes (%)
100
80
60
40
20
0
ns
Low ΔΨm
High ΔΨm
T-bet (%)
100
80
60
40
20
0
ns
Low ΔΨm
High ΔΨm

Extended data Fig. 3

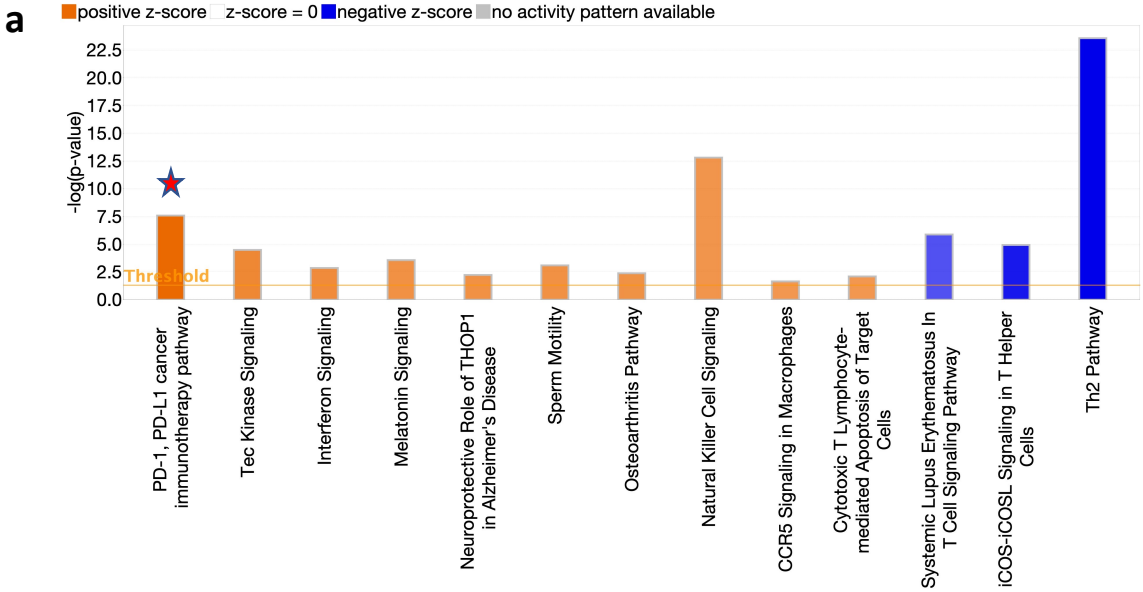

Fig. 4

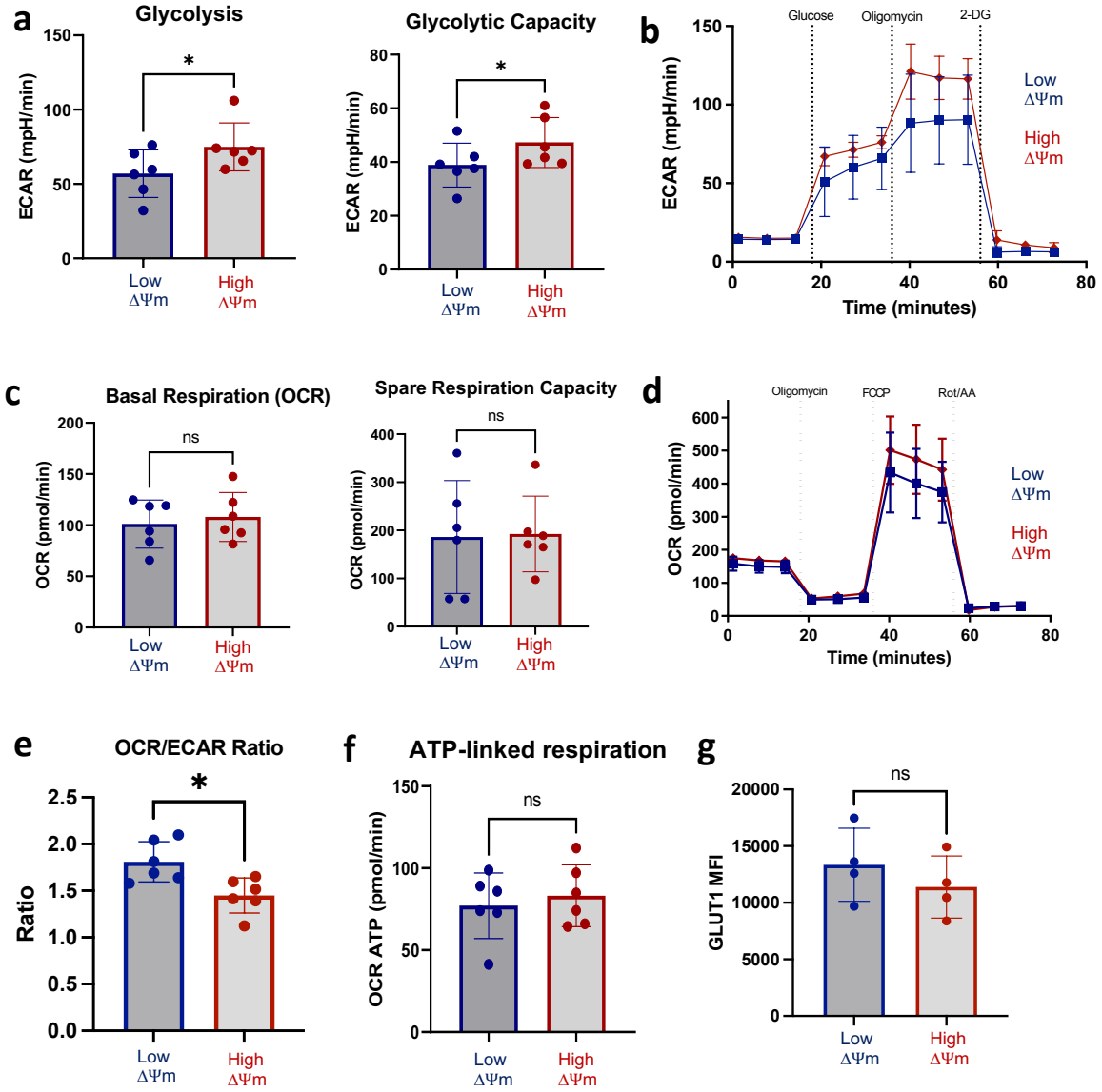
a
Glycolysis
ECAR (mpH/min)
150
100
50
0
*
Low ΔΨm
High ΔΨm
Glycolytic Capacity
ECAR (mpH/min)
80
60
40
20
0
*
Low ΔΨm
High ΔΨm
b
Glucose
Oligomycin
2-DG
ECAR (mpH/min)
150
100
50
0
Low ΔΨm
High ΔΨm
0
20
40
60
80
Time (minutes)
c
Basal Respiration (OCR)
OCR (pmol/min)
200
150
100
50
0
ns
Low ΔΨm
High ΔΨm
Spare Respiration Capacity
OCR (pmol/min)
400
300
200
100
0
ns
Low ΔΨm
High ΔΨm
d
Oligomycin
FCCP
Rot/AA
OCR (pmol/min)
600
500
400
300
200
100
0
Low ΔΨm
High ΔΨm
0
20
40
60
80
Time (minutes)
e
OCR/ECAR Ratio
Ratio
2.5
2.0
1.5
1.0
0.5
0.0
*
Low ΔΨm
High ΔΨm
f
ATP-linked respiration
OCR ATP (pmol/min)
150
100
50
0
ns
Low ΔΨm
High ΔΨm
g
GLUT1 MFI
20000
15000
10000
5000
0
ns
Low ΔΨm
High ΔΨm

Fig. 5

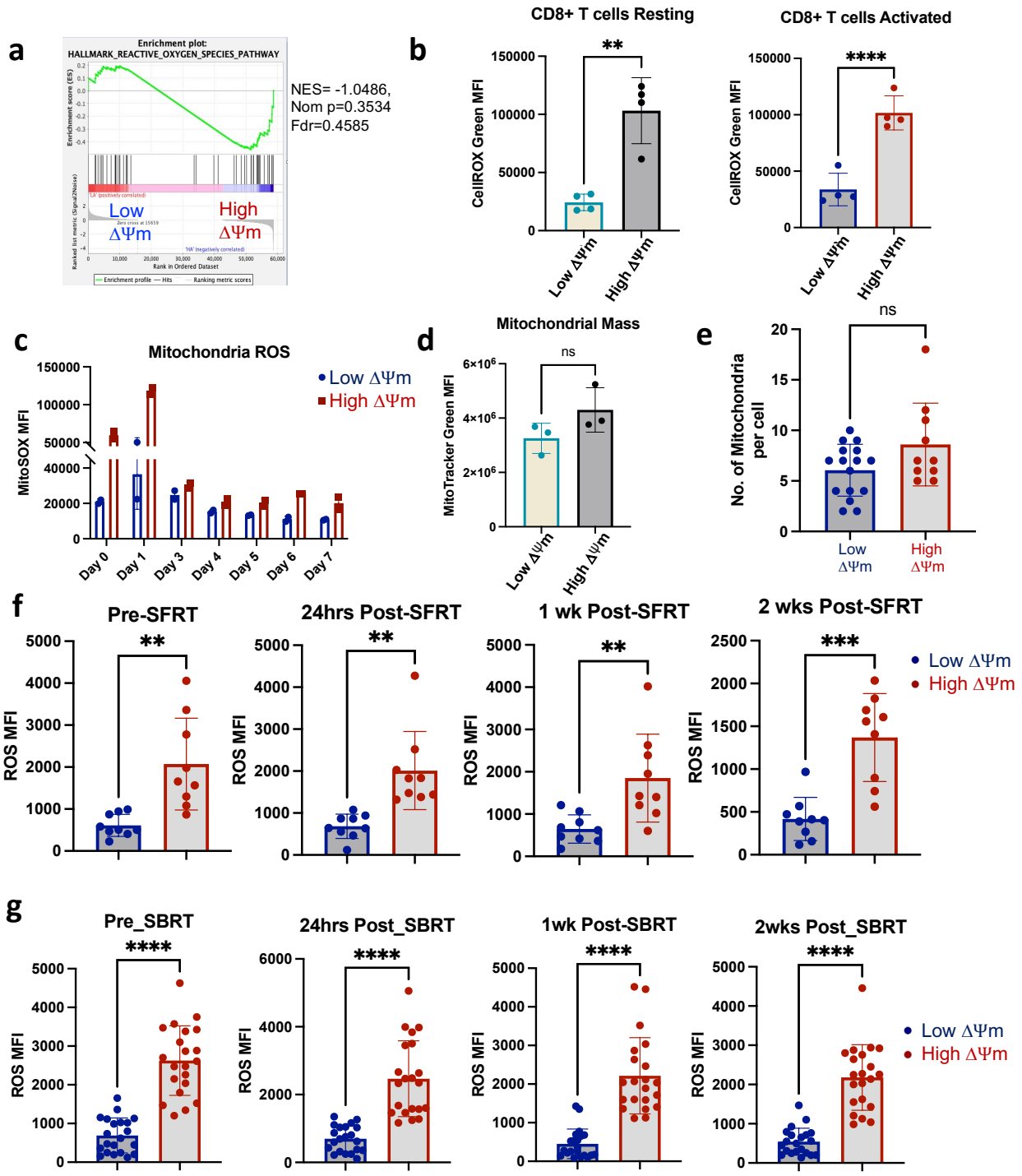
a
Enrichment plot:
HALLMARK_REACTIVE_OXYGEN_SPECIES_PATHWAY
NES= -1.0486,
Nom p=0.3534
Fdr=0.4585
Low ΔΨm
High ΔΨm
b
CD8+ T cells Resting
CD8+ T cells Activated
CellROX Green MFI
Low ΔΨm
High ΔΨm
c
Mitochondria ROS
MitoSOX MFI
Low ΔΨm
High ΔΨm
Day 0
Day 1
Day 3
Day 4
Day 5
Day 6
Day 7
d
Mitochondrial Mass
MitoTracker Green MFI
ns
e
No. of Mitochondria per cell
ns
f
Pre-SFRT
24hrs Post-SFRT
1 wk Post-SFRT
2 wks Post-SFRT
ROS MFI
Low ΔΨm
High ΔΨm
g
Pre_SBRT
24hrs Post_SBRT
1wk Post-SBRT
2wks Post_SBRT
ROS MFI
Low ΔΨm
High ΔΨm

Fig. 6

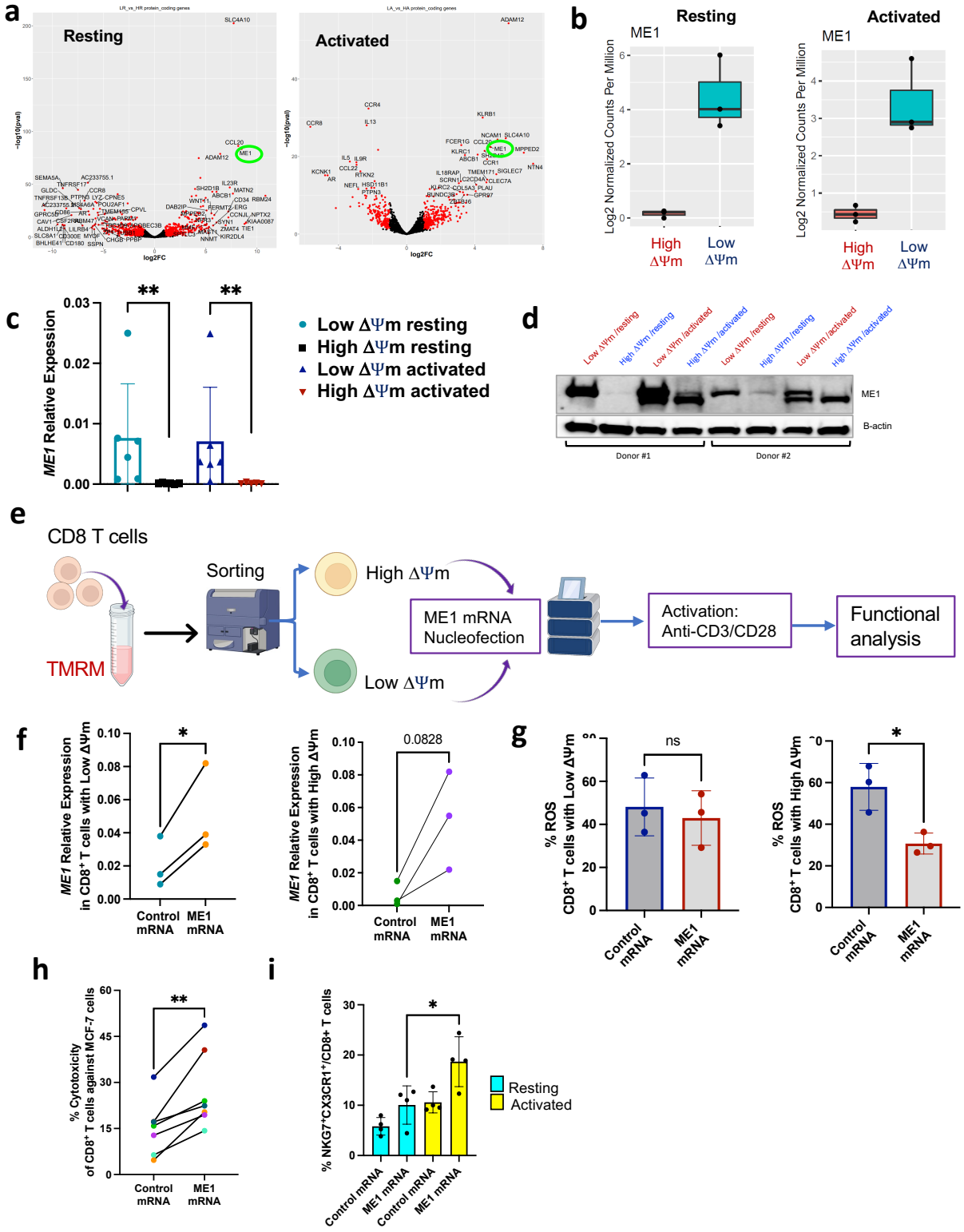
a
Resting
Activated
log2FC
b
Resting
Activated
ME1
Log2 Normalized Counts Per Million
High ΔΨm
Low ΔΨm
c
ME1 Relative Expression
Low ΔΨm resting
High ΔΨm resting
Low ΔΨm activated
High ΔΨm activated
d
Low ΔΨm /resting
High ΔΨm /resting
Low ΔΨm /activated
High ΔΨm /activated
ME1
B-actin
Donor #1
Donor #2
e
CD8 T cells
TMRM
Sorting
High ΔΨm
Low ΔΨm
ME1 mRNA Nucleofection
Activation: Anti-CD3/CD28
Functional analysis
f
ME1 Relative Expression in CD8+ T cells with Low ΔΨm
ME1 Relative Expression in CD8+ T cells with High ΔΨm
0.0828
Control mRNA
ME1 mRNA
g
% ROS CD8+ T cells with Low ΔΨm
% ROS CD8+ T cells with High ΔΨm
ns
h
% Cytotoxicity of CD8+ T cells against MCF-7 cells
i
% NKG7+CX3CR1+/CD8+ T cells
Resting
Activated

Fig. 7

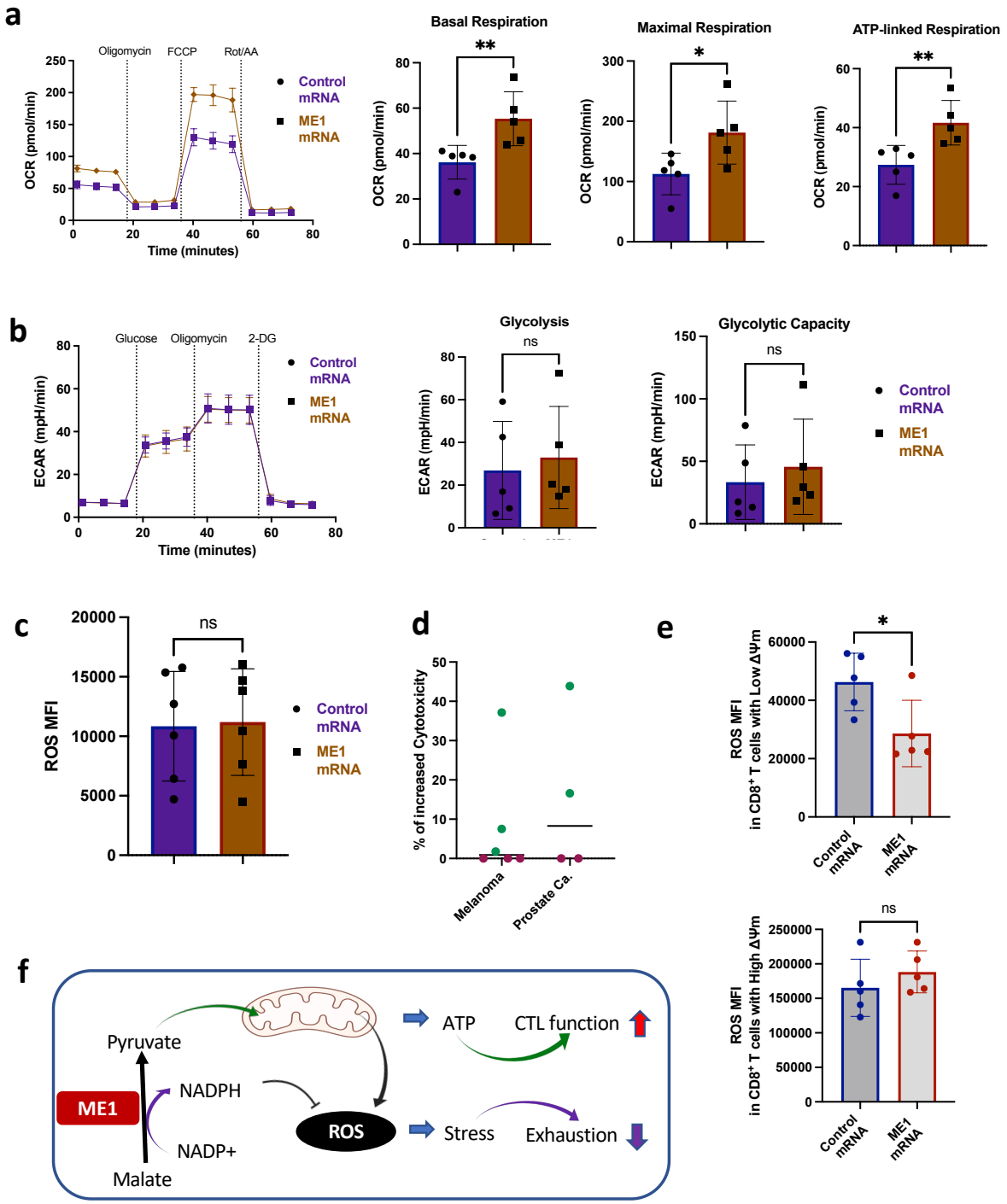
a
Oligomycin
FCCP
Rot/AA
OCR (pmol/min)
Time (minutes)
Control mRNA
ME1 mRNA
Basal Respiration
Maximal Respiration
ATP-linked Respiration
**
*
**
b
Glucose
Oligomycin
2-DG
ECAR (mpH/min)
Time (minutes)
Glycolysis
Glycolytic Capacity
ns
ns
c
ROS MFI
ns
d
% of increased Cytotoxicity
Melanoma
Prostate Ca.
e
ROS MFI in CD8+ T cells with Low ΔΨm
*
ROS MFI in CD8+ T cells with High ΔΨm
ns
Control mRNA
ME1 mRNA
f
Pyruvate
ME1
NADPH
NADP+
Malate
ROS
ATP
CTL function
Stress
Exhaustion
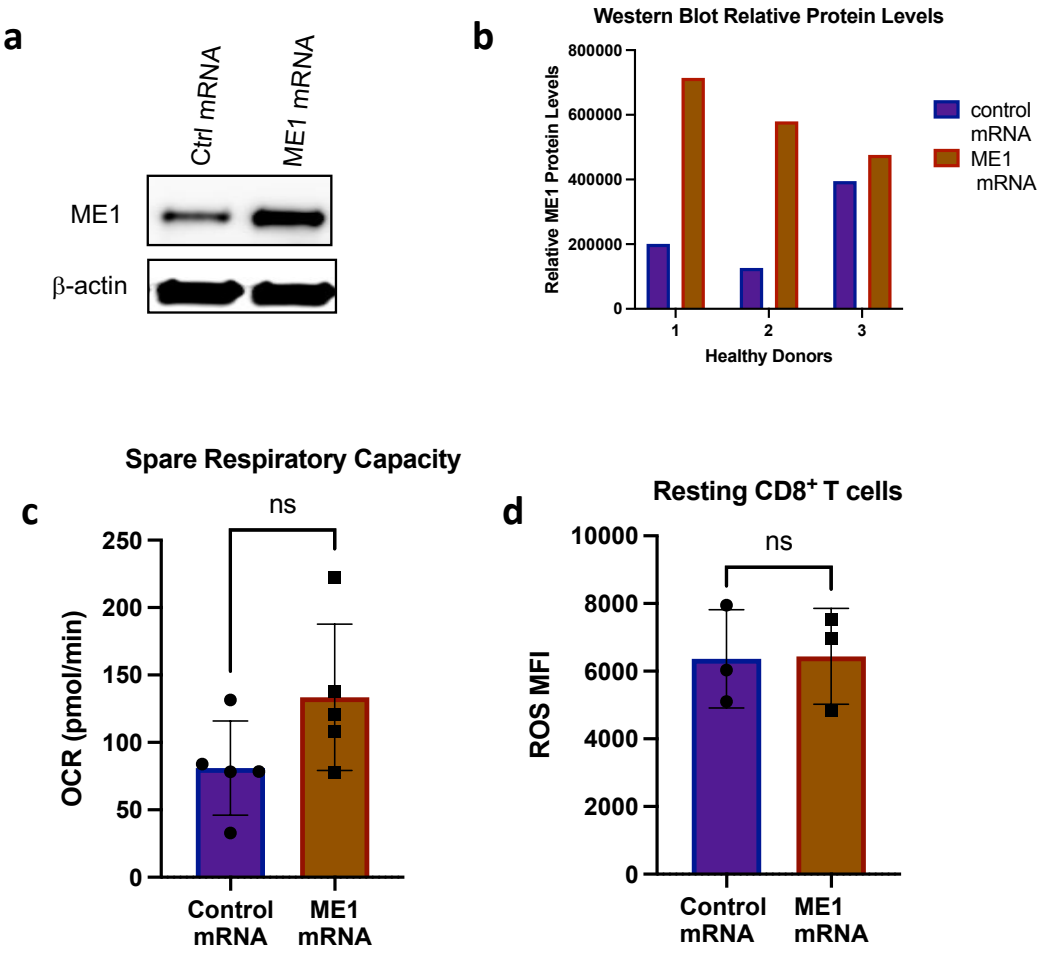
Extended data Fig. 4